Supplement of Atmos. Meas. Tech., 19, 333–358, 2026
https://doi.org/10.5194/amt-19-333-2026-supplement

Atmospheric Measurement Techniques
Open Access

Supplement of

Quantifying CH_4 point source emissions with airborne remote sensing: first results from AVIRIS-4

Sandro Meier et al.

Correspondence to: Sandro Meier (sandro.meier@empa.ch) and Gerrit Kuhlmann (gerrit.kuhlmann@empa.ch)

Supplement

Supplementary figures for MF vs LMF

The MF is based on the linearisation of the Beer-Lambert law. The linearisation error for the MF can be computed as follows:

$$L_{exact}(\lambda) = L_0(\lambda) \cdot e^{-\tau(\lambda)} \quad (S1)$$

Here, we use $\tau(\lambda) = \alpha \cdot s(\lambda)$, assuming that the optical depth linearly depends on the CH_4 enhancement. This assumption is justified when using a high-resolution input absorption spectrum $s(\lambda)$, for which individual absorption features are well resolved and saturation effects are negligible. This condition is satisfied for the spectrum employed in this study, which has a spectral resolution of 0.001 nm.

When linearising at $\alpha = 0$, we can approximate $L(\lambda)$:

$$L_{linear}(\lambda) = L_0(\lambda) \cdot \left(1 - \tau(\lambda)\right) \quad (S2)$$

The linearisation error is then calculated as

$$\delta L(\lambda) = L_{exact} - L_{linear}(\lambda) = L_0(\lambda) \cdot e^{-\tau(\lambda)} - L_0(\lambda) \cdot \left(1 - \tau(\lambda)\right) = L_0(\lambda) \cdot \left(e^{-\tau(\lambda)} - (1 - \tau)\right) \quad (S3)$$

Using the remainder of the Taylor series expansion, $\delta L(\lambda)$ can be approximated by

$$\delta L(\lambda) \approx L_0(\lambda) \cdot \frac{\tau^2}{2} \quad (S4)$$

However, when using our iterative approach to determine $s(\lambda)$, we no longer linearise at $\alpha = 0$ but at α_i:

$$L(\lambda) = L_0(\lambda) \cdot e^{-\alpha_i s} \quad (S5)$$

$$L_{\alpha_i}(\lambda) \approx L(\lambda) + \left.\frac{dL}{ds}\right|_{\alpha_i} (\alpha - \alpha_i) \quad (S6)$$

$$\left.\frac{dL}{ds}\right|_{\alpha_i} = -L_0(\lambda) \cdot \alpha_i \cdot e^{-\alpha_i s} \quad (S7)$$

$$L_{\alpha_i}(\lambda) \approx L(\lambda) - L_0(\lambda) \cdot \alpha_i \cdot e^{-\alpha_i s}(\alpha - \alpha_i) \quad (S8)$$

Therefore, the linearisation error at α_i becomes

$$\delta L(\lambda) = L(\lambda) - L_{\alpha_i}(\lambda) = L_0(\lambda) \cdot e^{-\alpha s} - \left(L_0(\lambda) \cdot e^{-\alpha_i s} - L_0(\lambda) \cdot \alpha_i \cdot e^{-\alpha_i s}(\alpha - \alpha_i)\right) \quad (S9)$$

Eq. S9 can be approximated using Taylor expansion as

$$\delta L(\lambda) \approx \frac{1}{2} \cdot L_0(\lambda) \cdot s_0^2 \cdot e^{-\alpha_i s}(\alpha - \alpha_i)^2 \quad (S10)$$

If we choose an α_i close to the true α, the error $\delta L(\lambda)$ goes towards 0.

To verify this, we generated a synthetic radiance dataset and embedded a CH_4 plume using the absorption spectrum of CH_4. Then, we applied the MF and LMF to this data. Figure S1 (a) shows the retrieved mean CH_4 enhancements within the plume using the MF and LMF. It can be seen that both the MF and LMF yield comparable results but the MF tends to slightly underestimate the emissions for higher enhancements. This is not only the result of the remainder of the linearisation error but a contamination of the mean spectrum for plumes with higher enhancements. This is shown in Figure S1 (b), which presents estimated CH_4 enhancements for a case with true enhancements of 20 ppm as a function of the fraction of the scene containing a

CH_4 plume. For larger fractions, more of the CH_4 absorption signal "leaks" into the mean spectrum and leads to an underestimation of the CH_4 enhancements. Conversely, due to the log transformation of the radiance data, the LMF is much more robust to this contamination. In the case of our study, the contamination likely

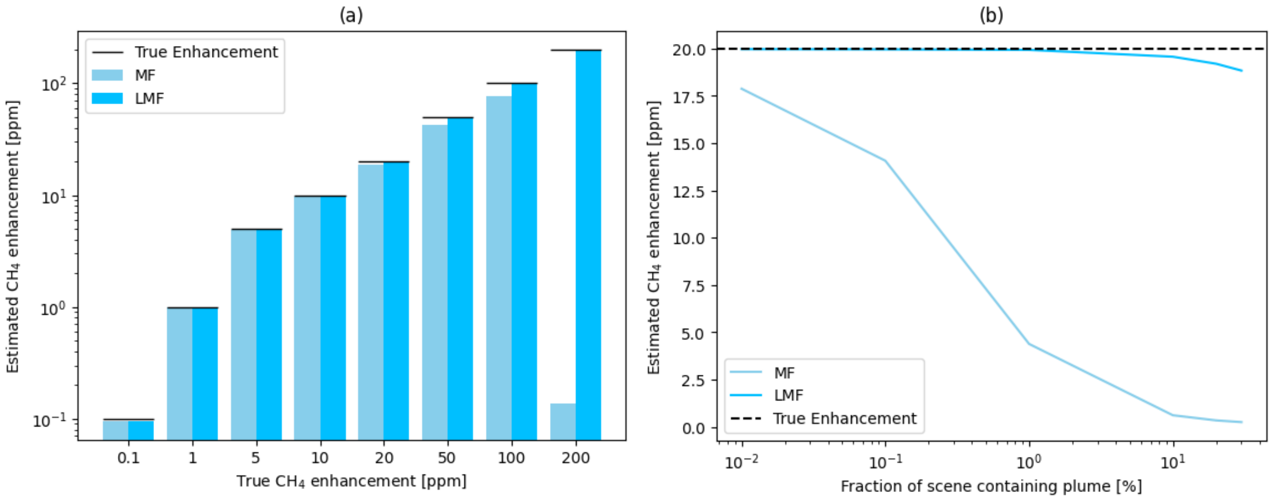

Figure S1: Comparison of CH_4 enhancements from MF and LMF for synthetic data. (a) Estimated CH_4 enhancement using MF and LMF. (b) Dependence of estimated CH_4 enhancement for increasing fractions of the scene containing a plume with a true CH_4 enhancement of 20ppm.

does not have a significant influence on the retrieved CH_4 enhancements as the mean is calculated over >23000 pixels in along-track direction whereas the plumes only consist of a few dozen pixels, i.e. <0.05% of the scene. Additionally, the strongest release only had mean CH_4 enhancements below 20 ppm.

Supplementary figures for emission estimates

This document contains overview figures for all emission estimates from AVIRIS-4 data of the controlled release experiment in September 2024 in Pau, France. The figures were produced using the Python library for data-driven emission quantification *ddeq* (version 1.0) which is available on Gitlab.com.

The retrieved AVIRIS-4 CH_4 maps, wind and sources data as well as estimated emissions are available on the Zenodo data repository (DOI: 10.5281/zenodo.16410532).

Data and images of each overpass share the following naming convention:

M0{*CampaignDay*}_{*YYMMDD*}_FRA_Pau_Methane_{*Altitude*}ft_Line_{*Orientation*}_{*HHMMSS*}_000_rdn{*Suffix*}

- Orientation: "0002" and "20001" are overpasses in E-W direction and "0001" and "10001" in N-S direction
- Suffix: depends on the data product and can be "winds", "sources", "{*method*}_data", "{*method*}_results" or "{*method*}_emissions"

The results figure of the cross-sectional flux method consists of four subplots

a. RGB image of the release site
b. CH_4 map with identified source location, detected plume and centre line
c. Gaussian fits to the CH_4 columns from the first and last three cross-sections
d. Along-plume flux estimates of all cross-sections and retrieval metadata.

The results figure of the cross-sectional flux method consists of three subplots

a. RGB image of the release site
b. CH_4 map with identified source location, detected plume and centre line
c. Retrieval metadata.

The wind method "Effective wind" refers to the wind speed at source height described in Section 2.5.

Day 1: 16.09.2024

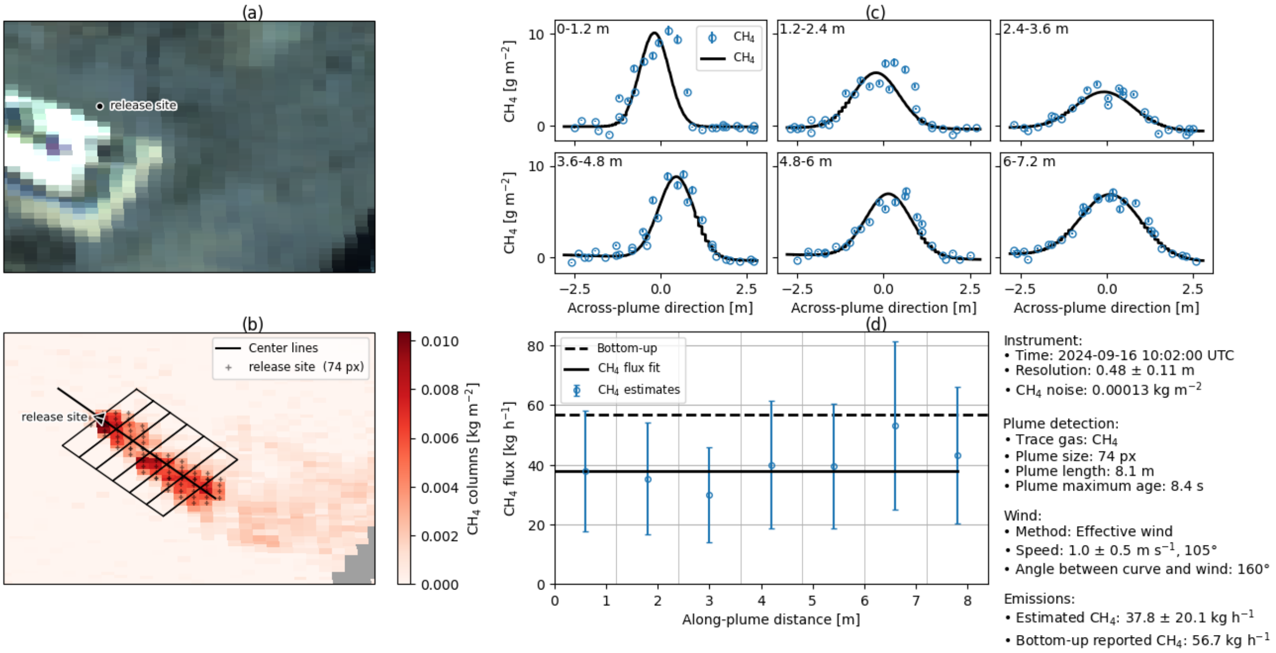

Fig. S2: M014_240916_FRA_Pau_Methane_4200ft_Line_0002_120230_000_rdn_csf_results

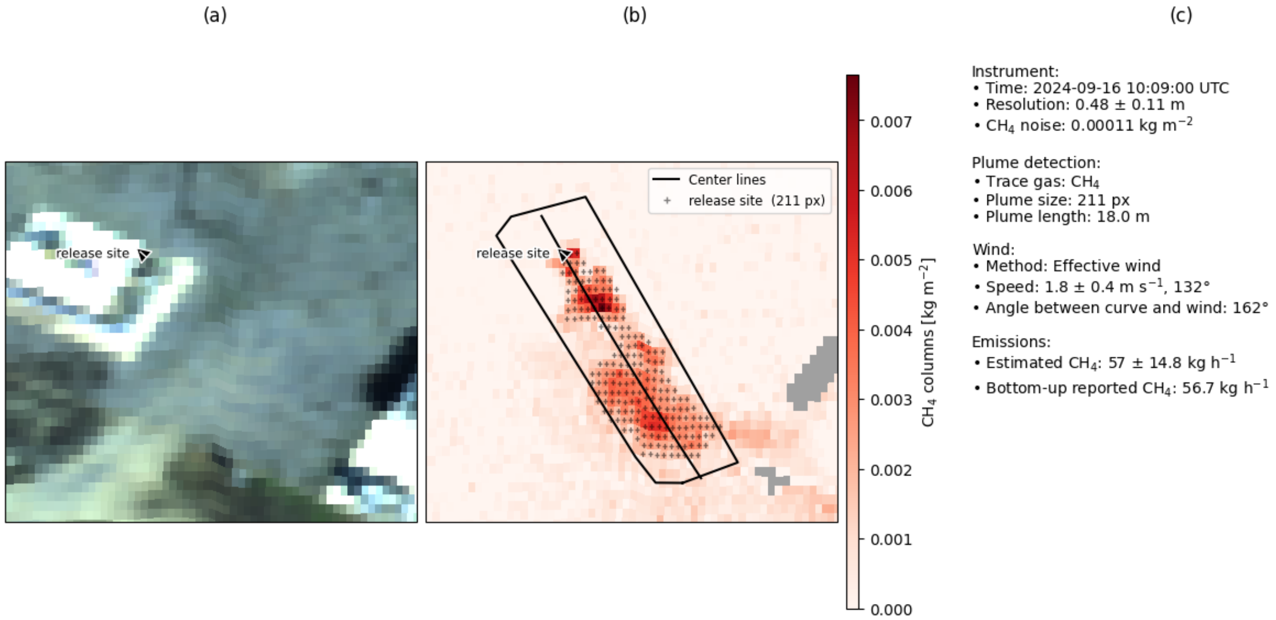

Fig. S3: M014_240916_FRA_Pau_Methane_4200ft_Line_0001_120919_000_rdn_ime_results

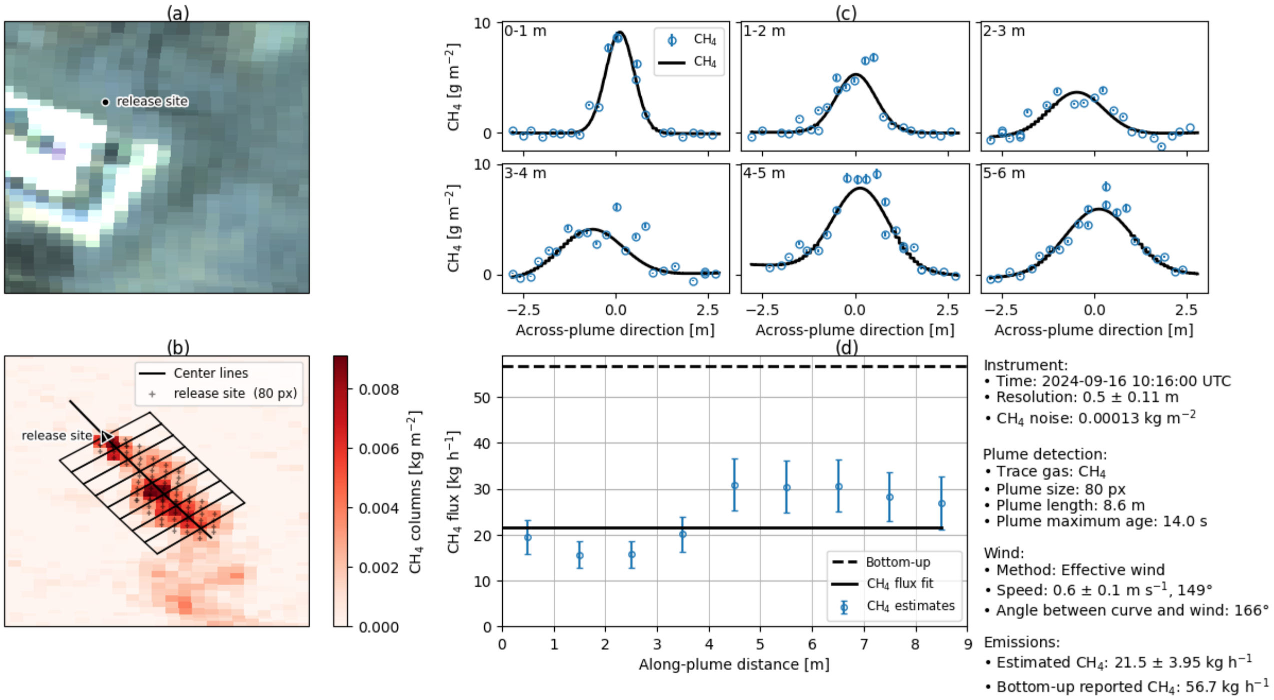

Fig. S4: M014_240916_FRA_Pau_Methane_4200ft_Line_0002_121538_000_rdn_csf_results

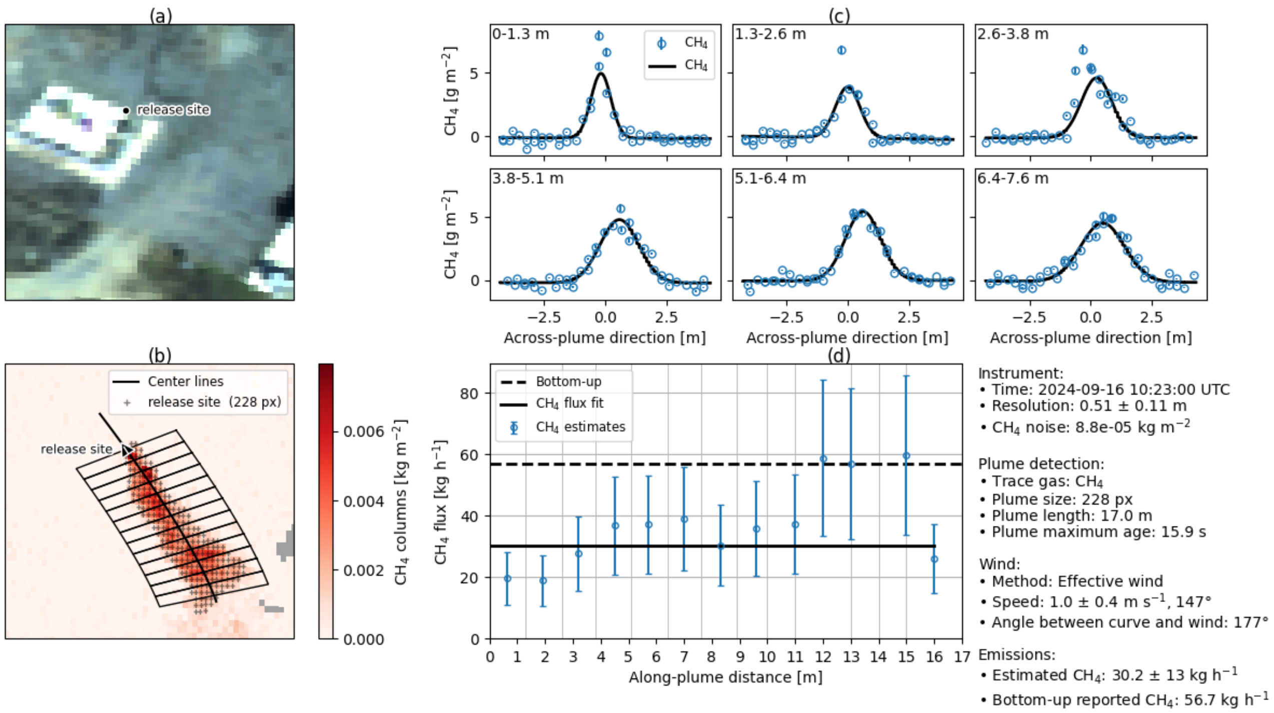

Fig. S5: M014_240916_FRA_Pau_Methane_4200ft_Line_0001_122236_000_rdn_csf_results

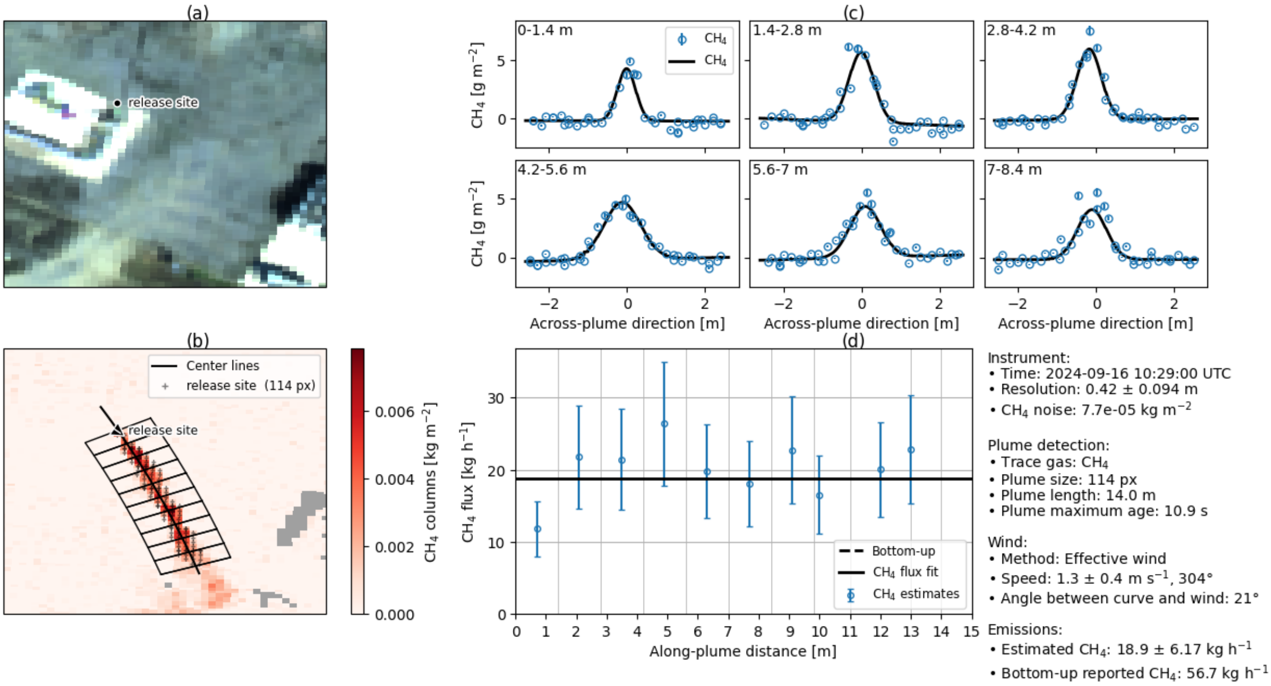

Fig. S6: M014_240916_FRA_Pau_Methane_3000ft_Line_0002_122920_000_rdn_csf_results

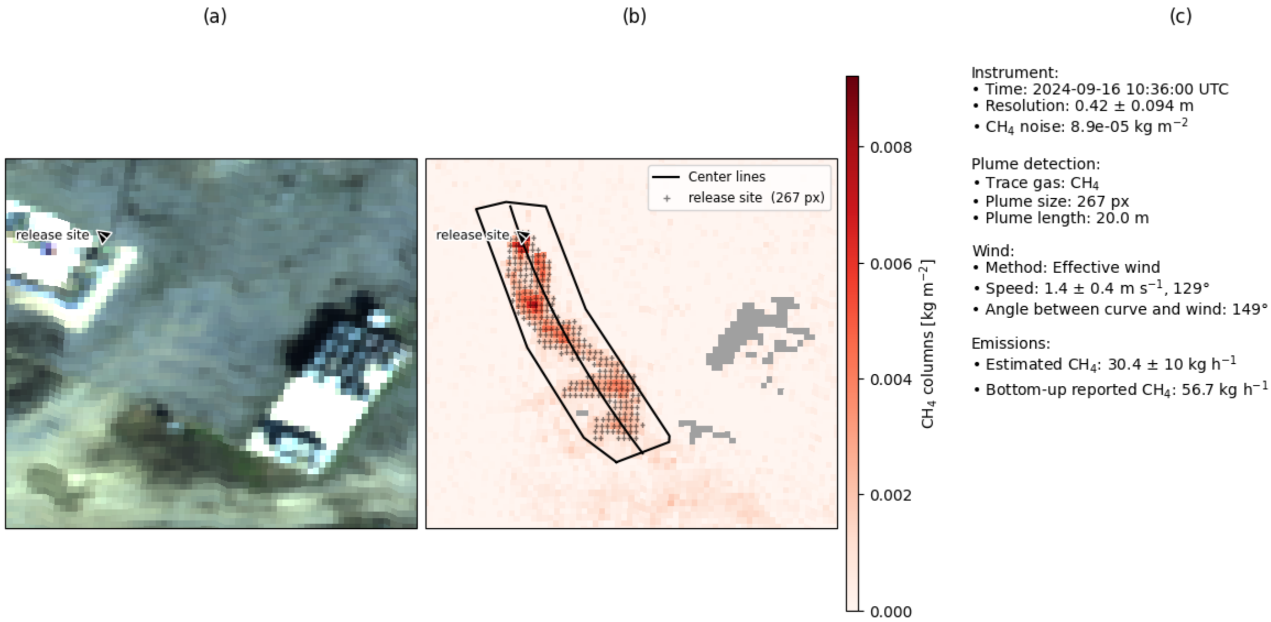

Fig. S7: M014_240916_FRA_Pau_Methane_3000ft_Line_0001_123559_000_rdn_ime_results

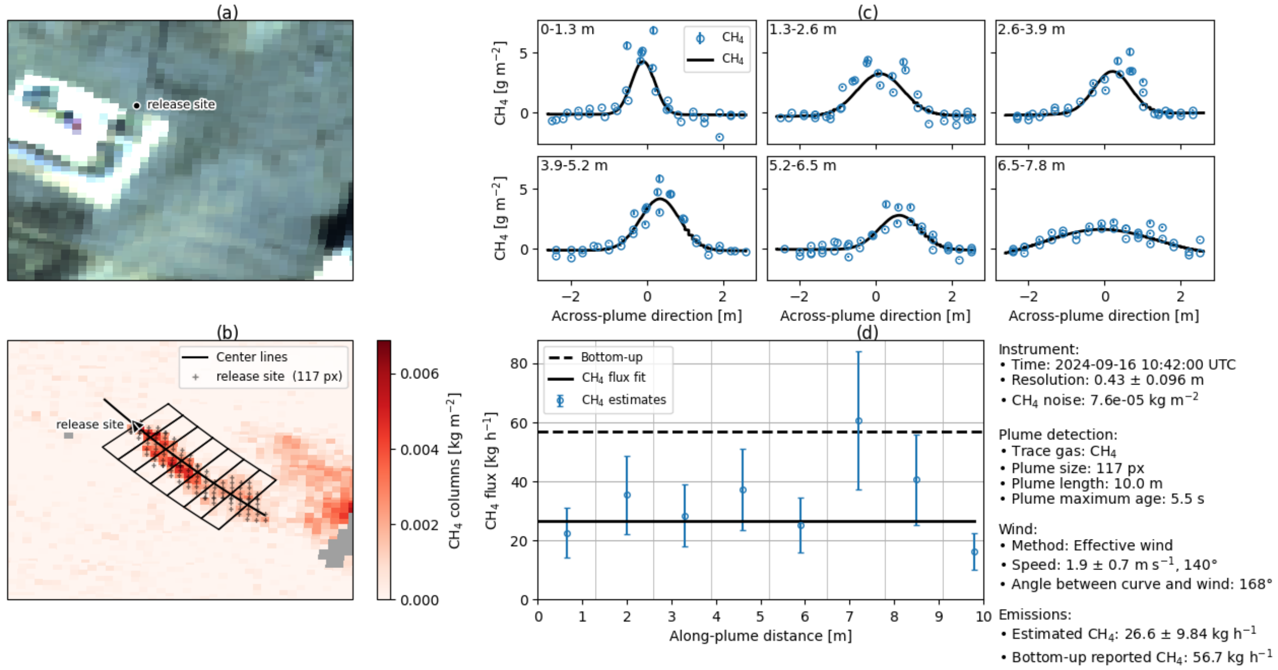

Fig. S8: M014_240916_FRA_Pau_Methane_3000ft_Line_0002_124215_000_rdn_csf_results

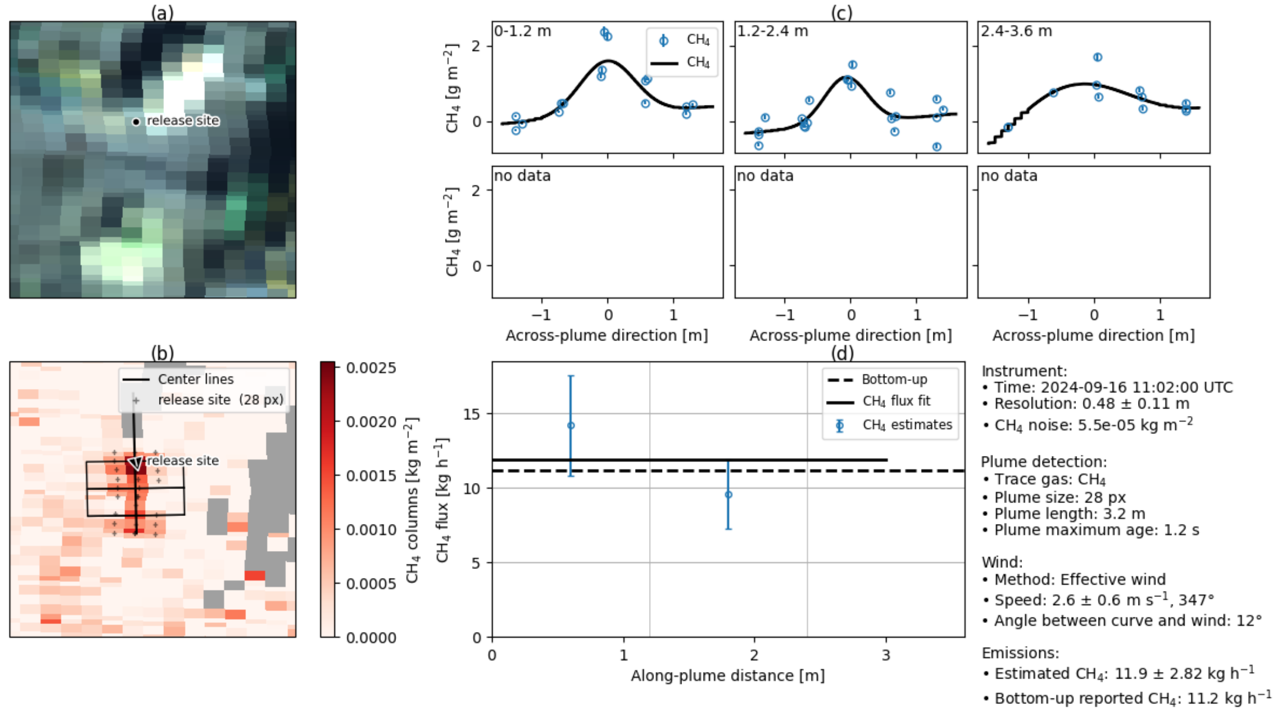

Fig. S9: M014_240916_FRA_Pau_Methane_4200ft_Line_0002_130225_000_rdn_csf_results

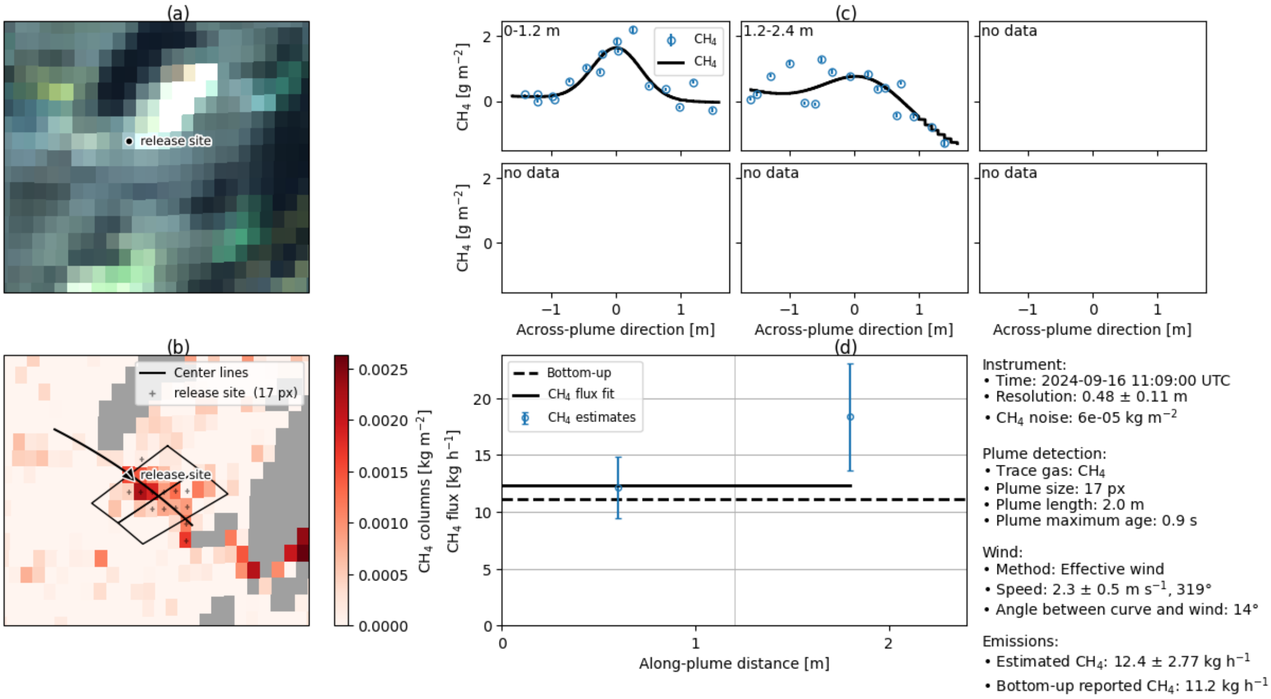

Fig. S10: M014_240916_FRA_Pau_Methane_4200ft_Line_0001_130856_000_rdn_csf_results

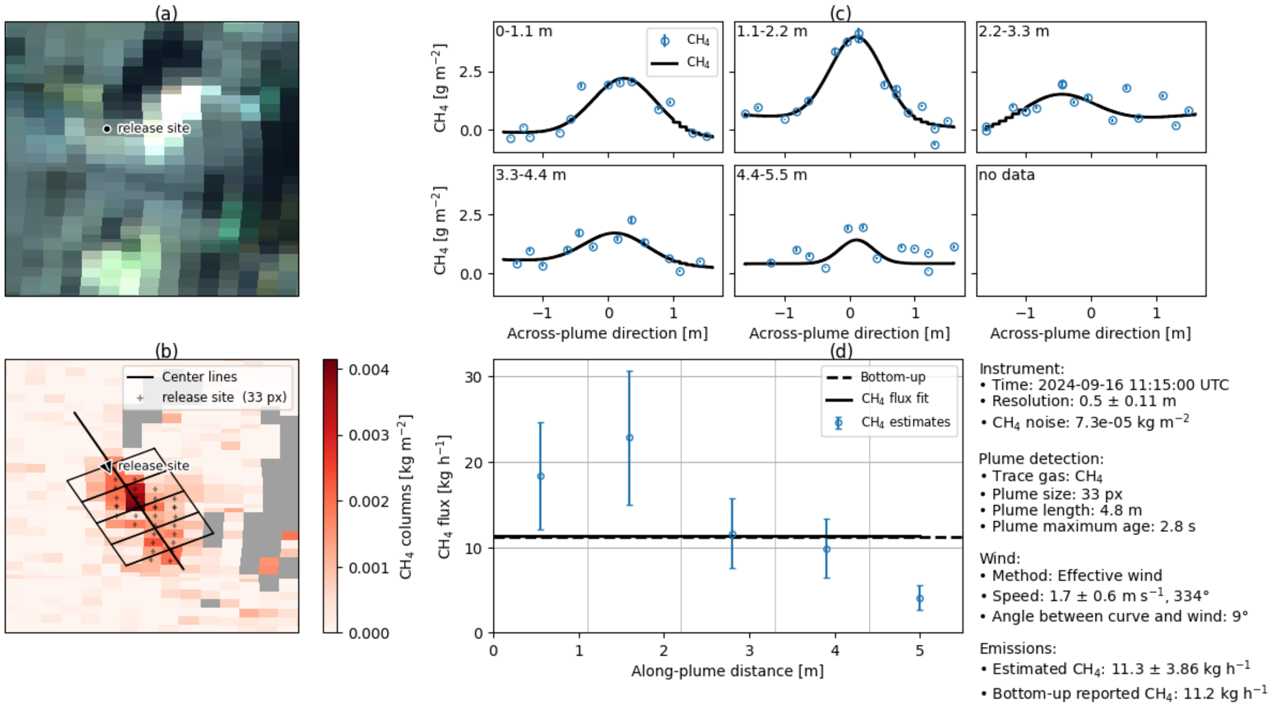

Fig. S11: M014_240916_FRA_Pau_Methane_4200ft_Line_0002_131436_000_rdn_csf_results

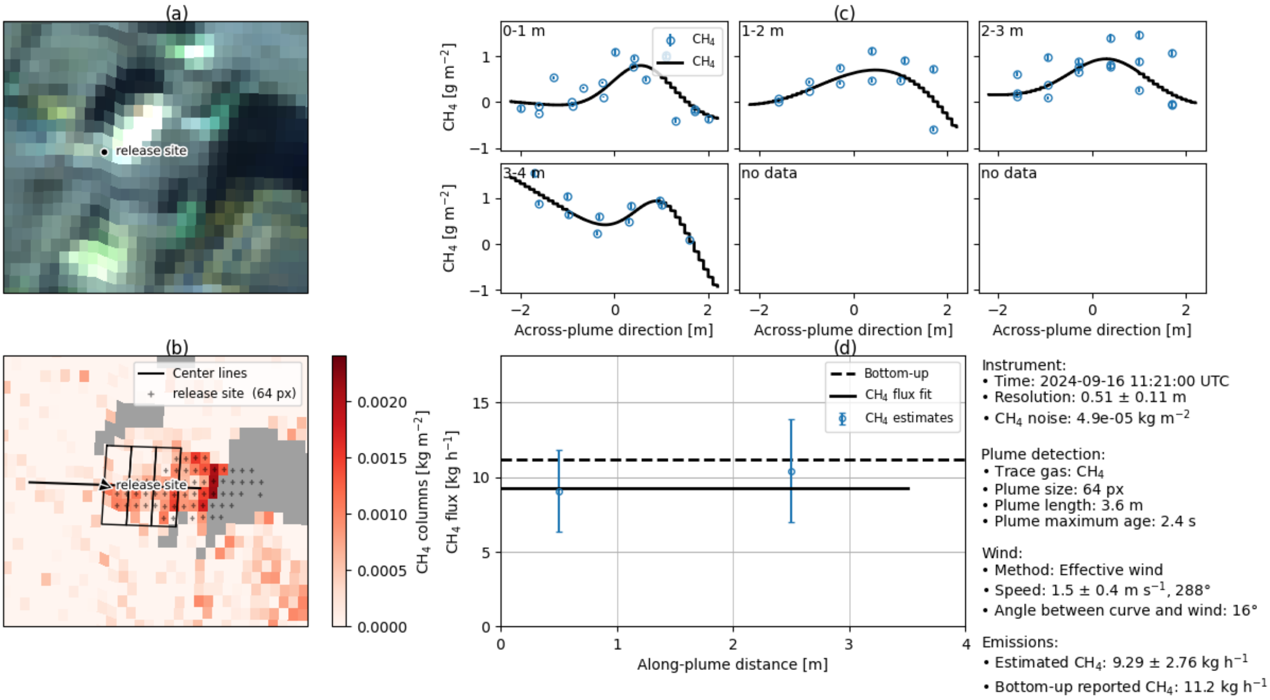

Fig. S12: M014_240916_FRA_Pau_Methane_4200ft_Line_0001_132059_000_rdn_csf_results

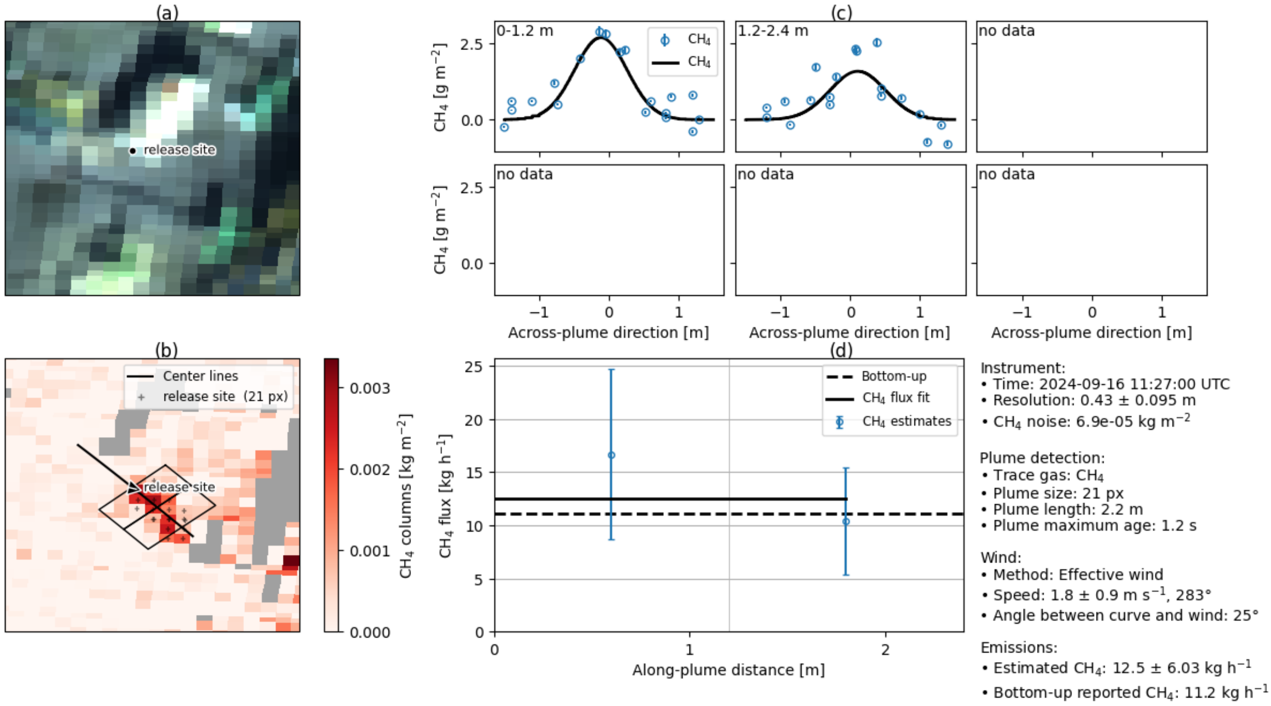

Fig. S13: M014_240916_FRA_Pau_Methane_3000ft_Line_0002_132711_000_rdn_csf_results

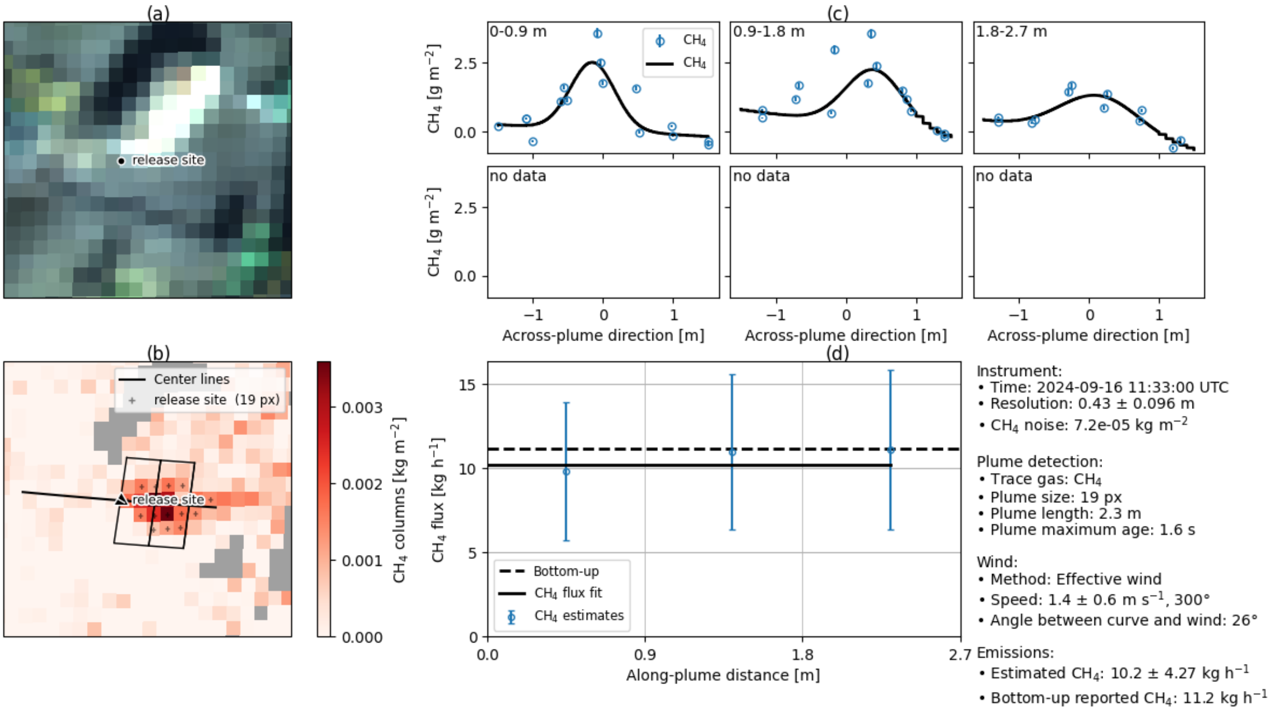

Fig. S14: M014_240916_FRA_Pau_Methane_3000ft_Line_0001_133313_000_rdn_csf_results

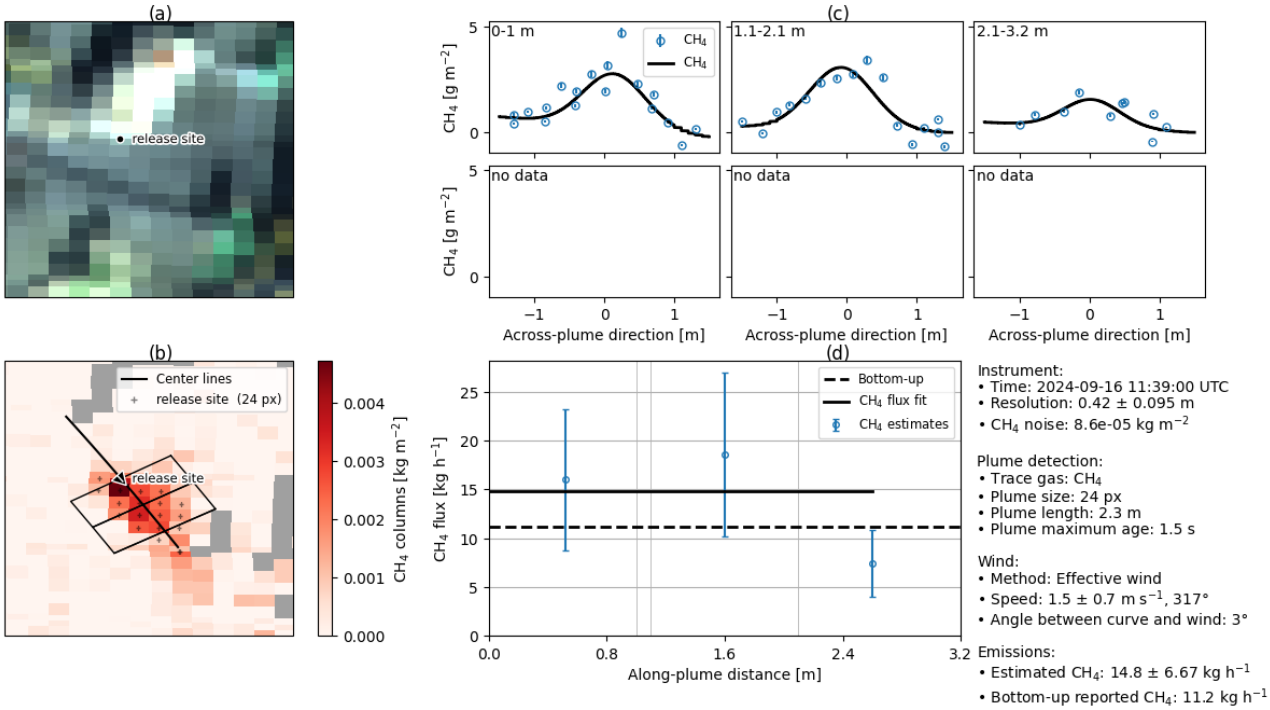

Fig. S15: M014_240916_FRA_Pau_Methane_3000ft_Line_0002_133911_000_rdn_csf_results

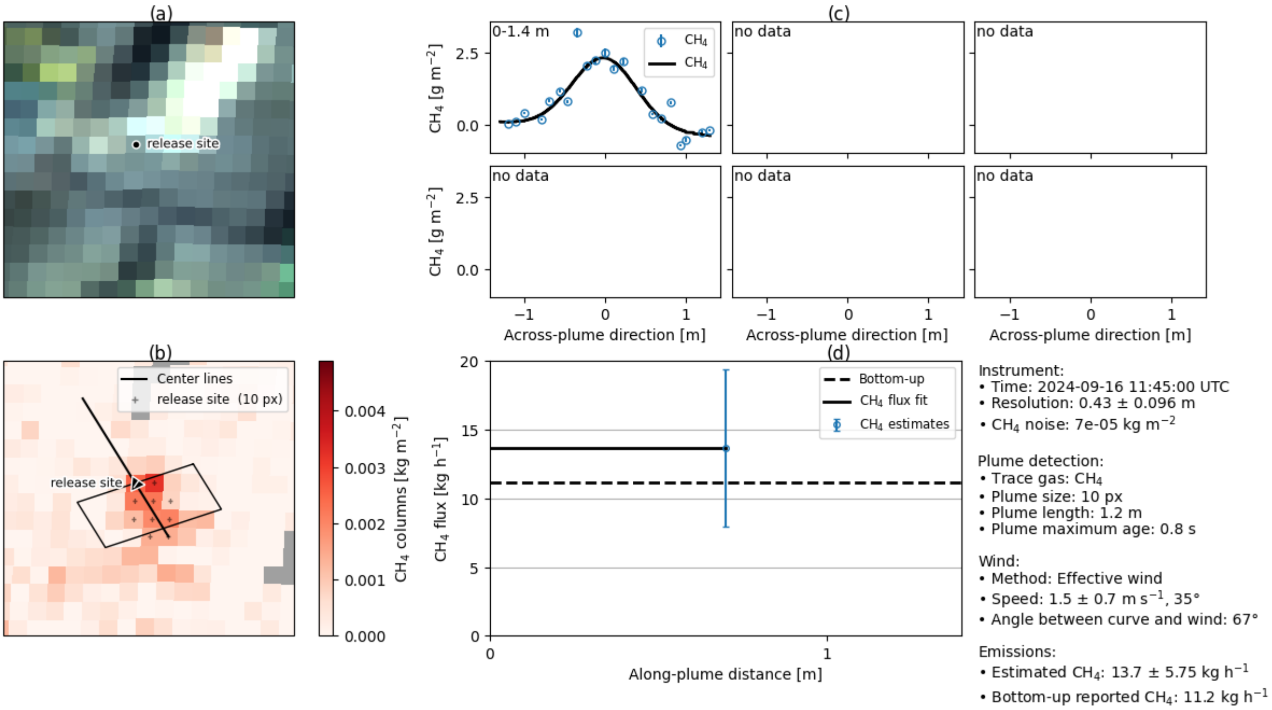

Fig. S16: M014_240916_FRA_Pau_Methane_3000ft_Line_0001_134509_000_rdn_csf_results

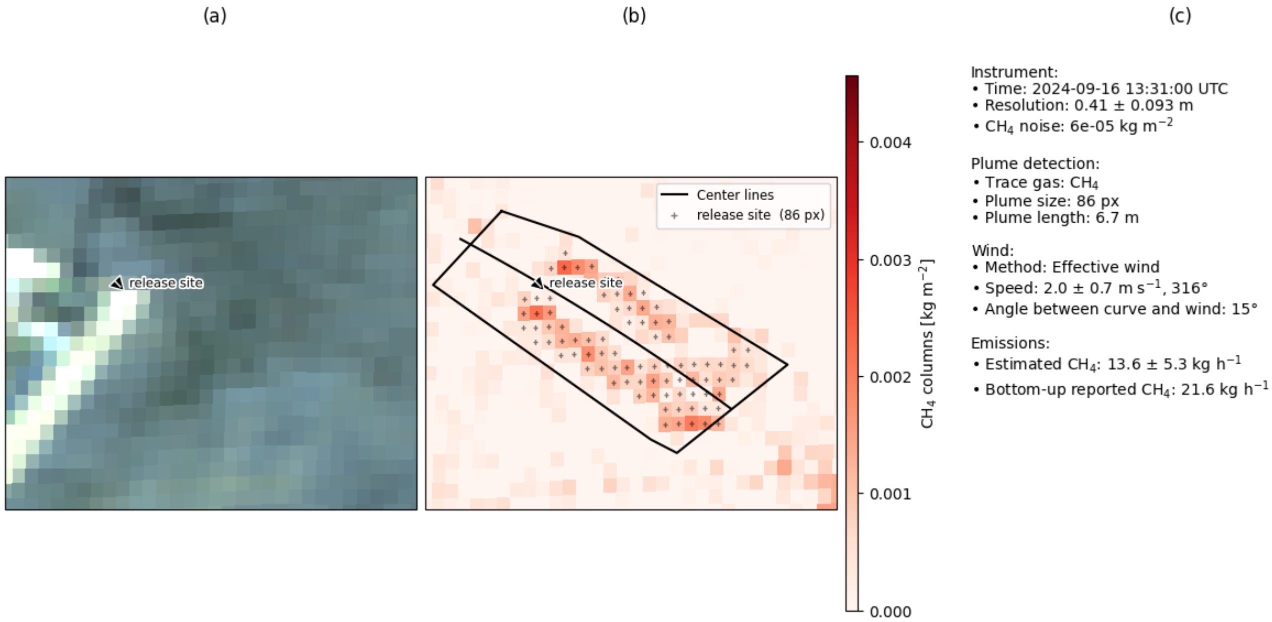

Fig. S17: M014_240916_FRA_Pau_Methane_3000ft_Line_0001_153045_000_rdn_ime_results

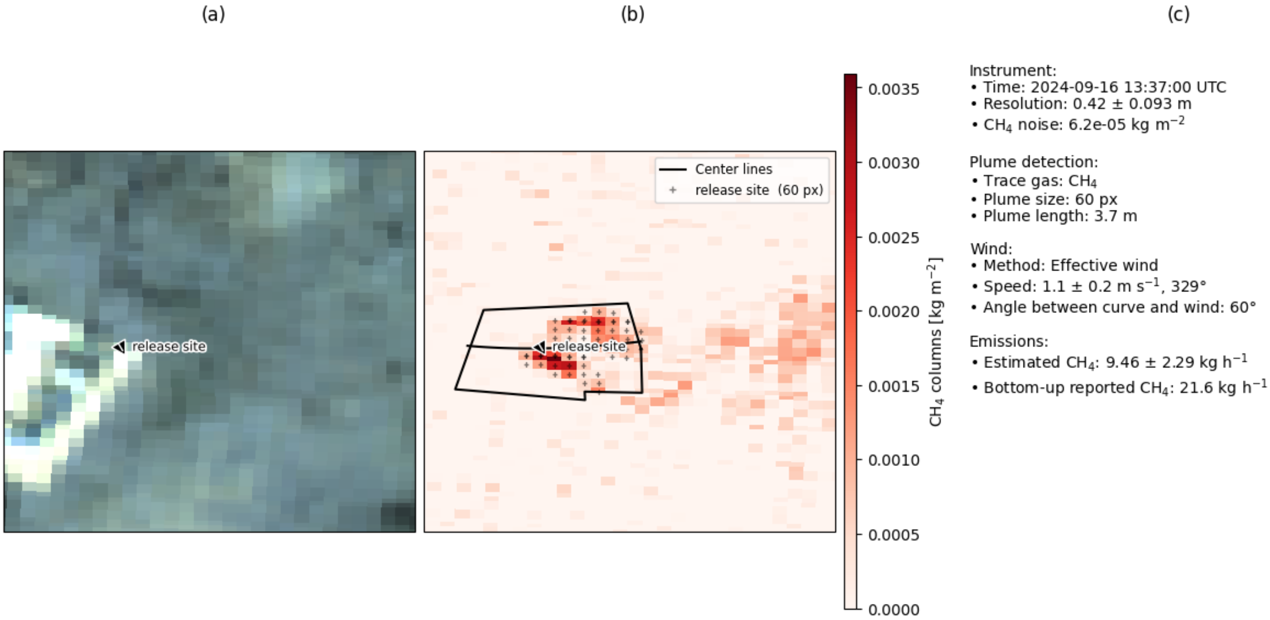

Fig. S18: M014_240916_FRA_Pau_Methane_3000ft_Line_0002_153716_000_rdn_ime_results

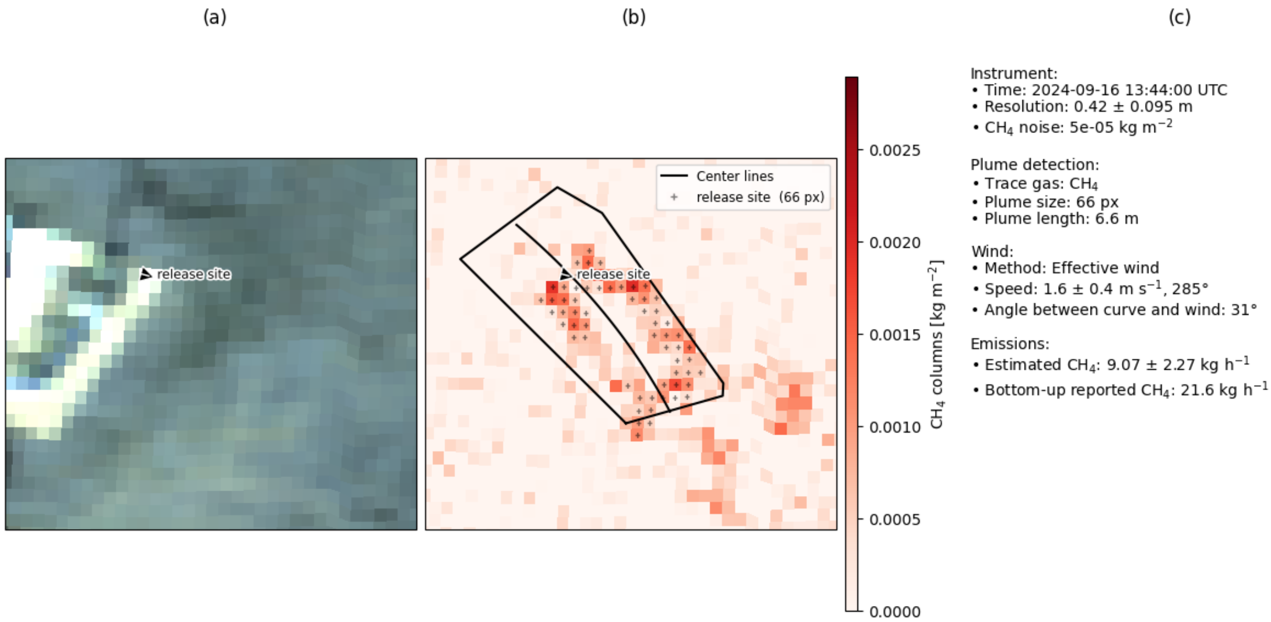

Fig. S19: M014_240916_FRA_Pau_Methane_3000ft_Line_0001_154350_000_rdn_ime_results

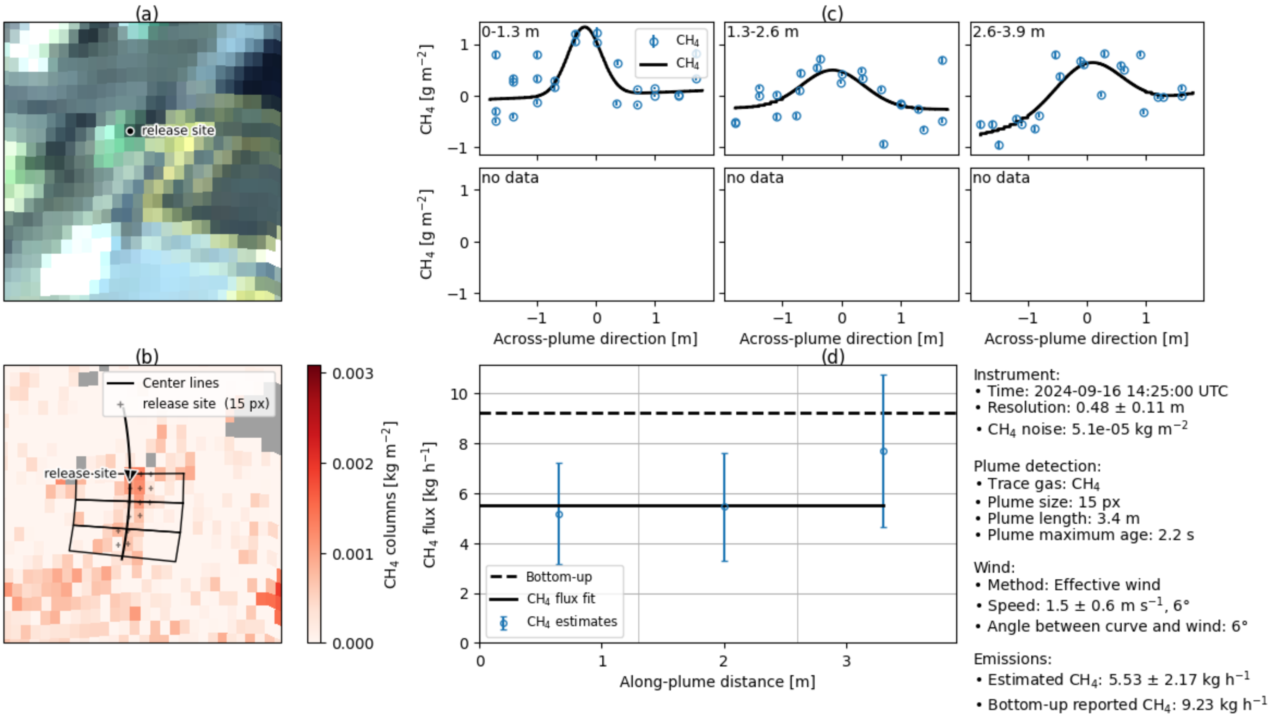

Fig. S20: M014_240916_FRA_Pau_Methane_4200ft_Line_0001_162509_000_rdn_csf_results

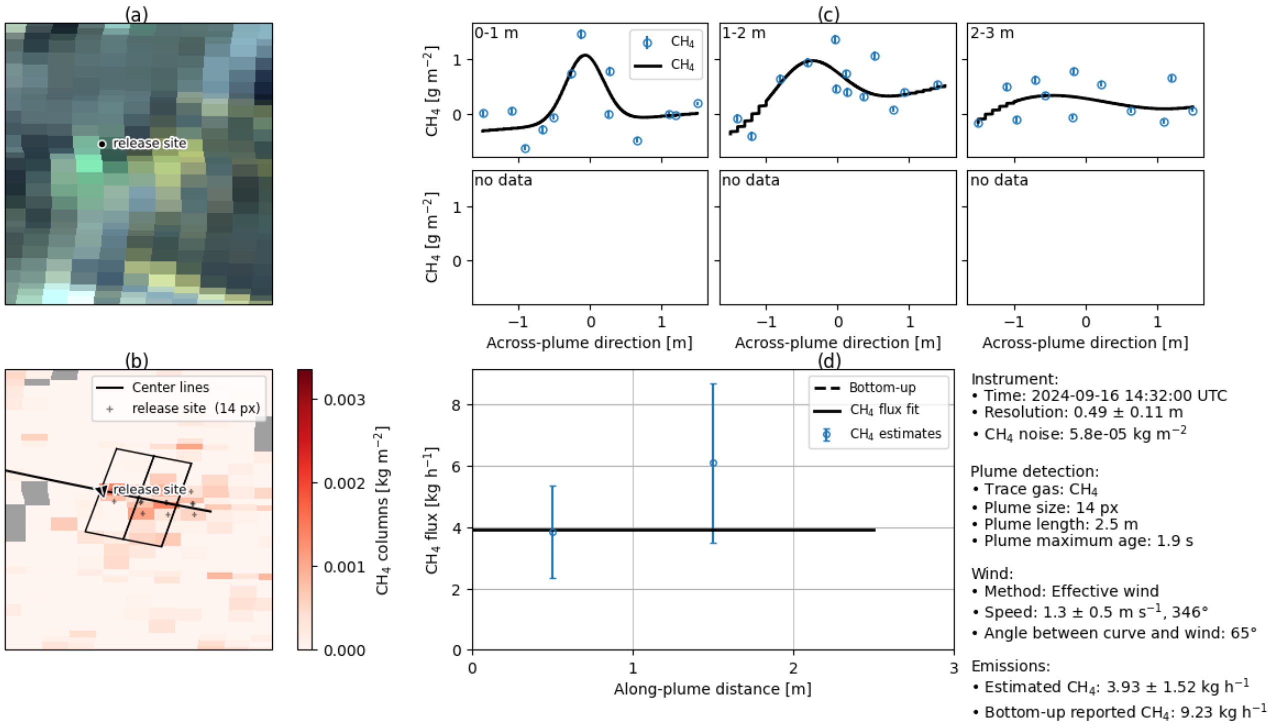

Fig. S21: M014_240916_FRA_Pau_Methane_4200ft_Line_0002_163136_000_rdn_csf_results

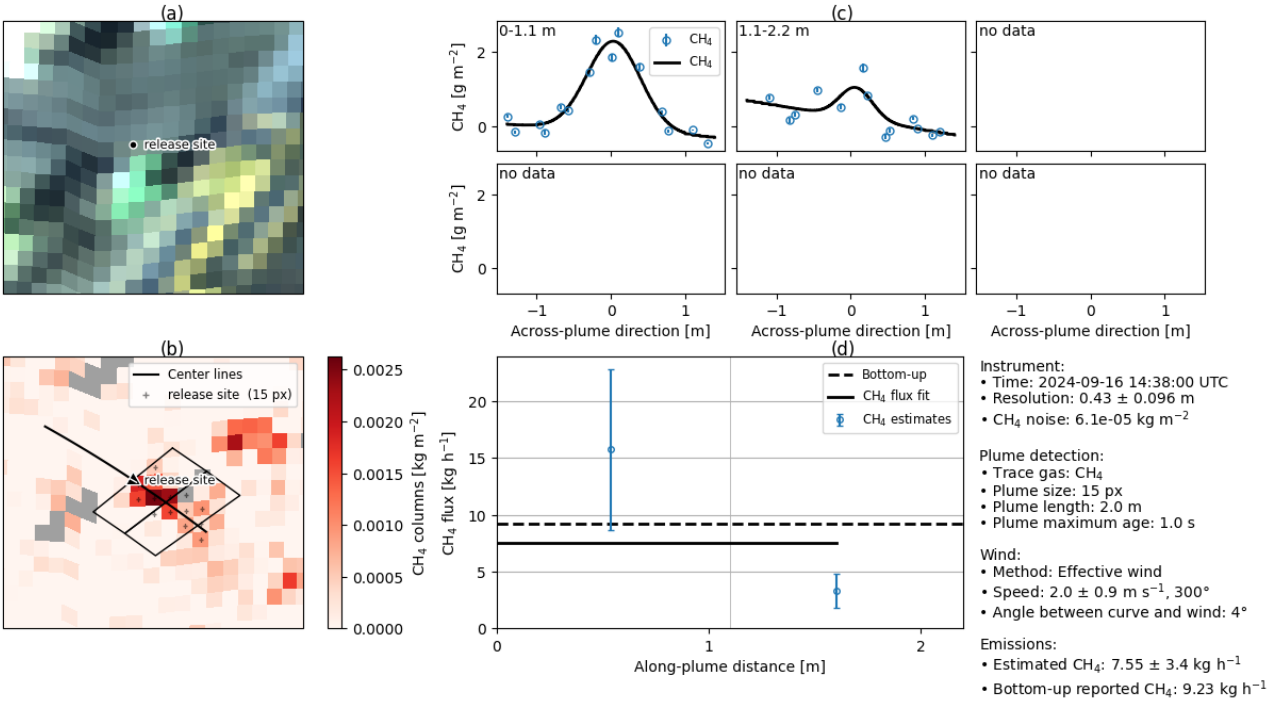

Fig. S22: M014_240916_FRA_Pau_Methane_3000ft_Line_0001_163819_000_rdn_csf_results

Day 2: 17.09.2024

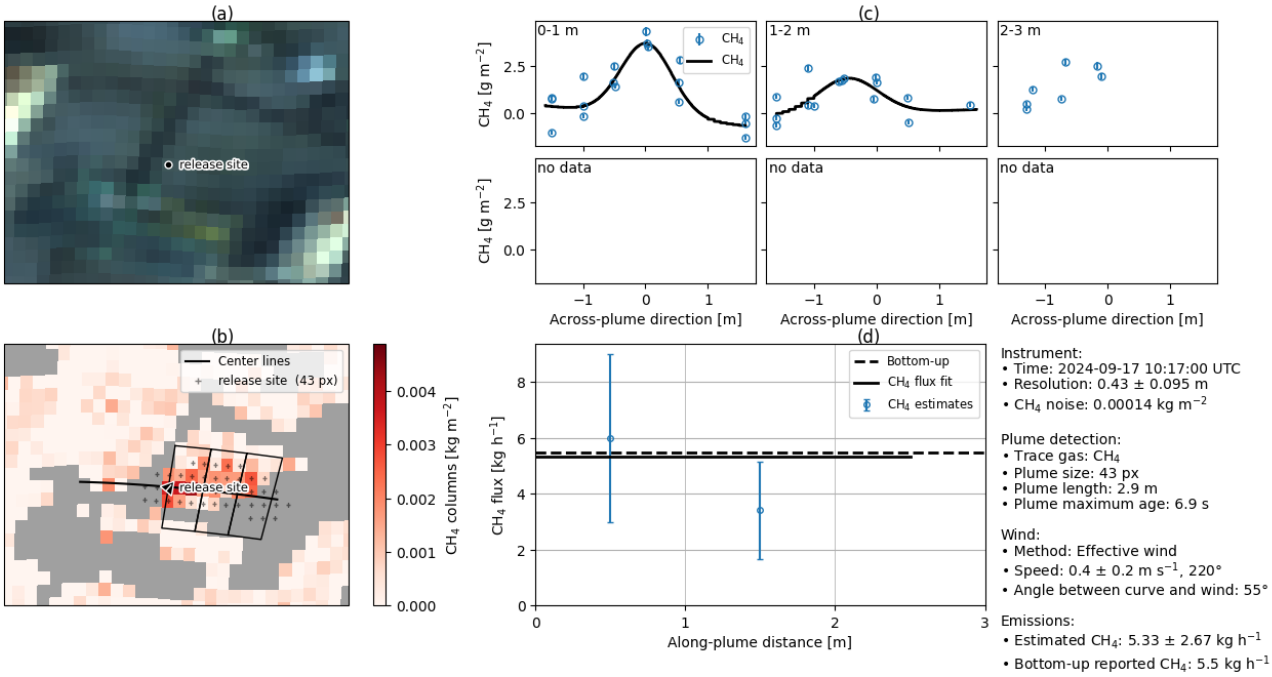

Fig. S23: M015_240917_FRA_Pau_Methane_3000ft_Line_10001_121704_000_rdn_csf_results

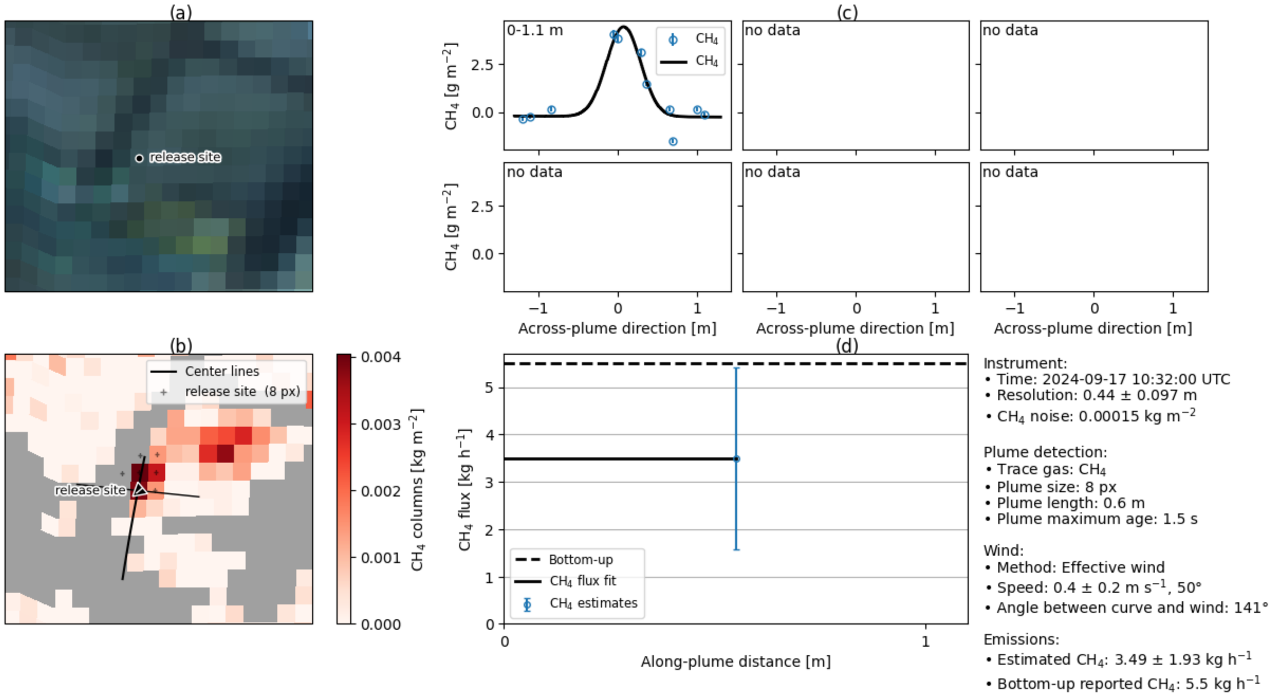

Fig. S24: M015_240917_FRA_Pau_Methane_3000ft_Line_10001_123130_000_rdn_csf_results

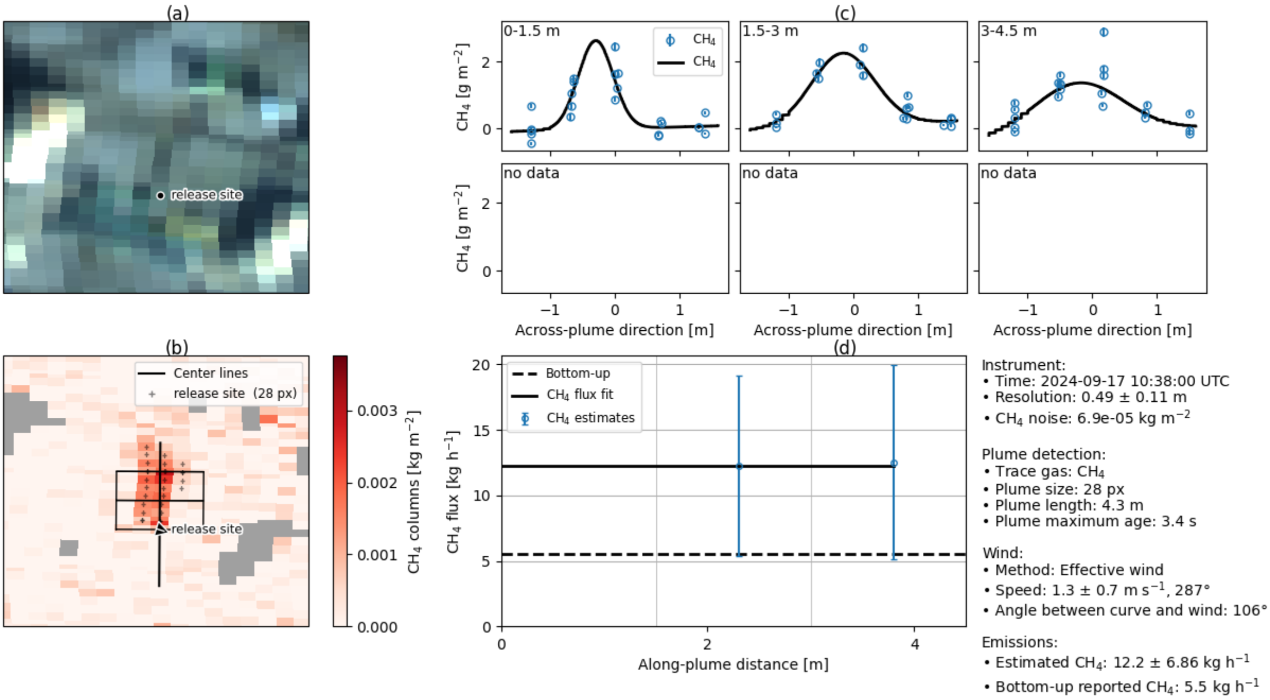

Fig. S25: M015_240917_FRA_Pau_Methane_4200ft_Line_20001_123734_000_rdn_csf_results

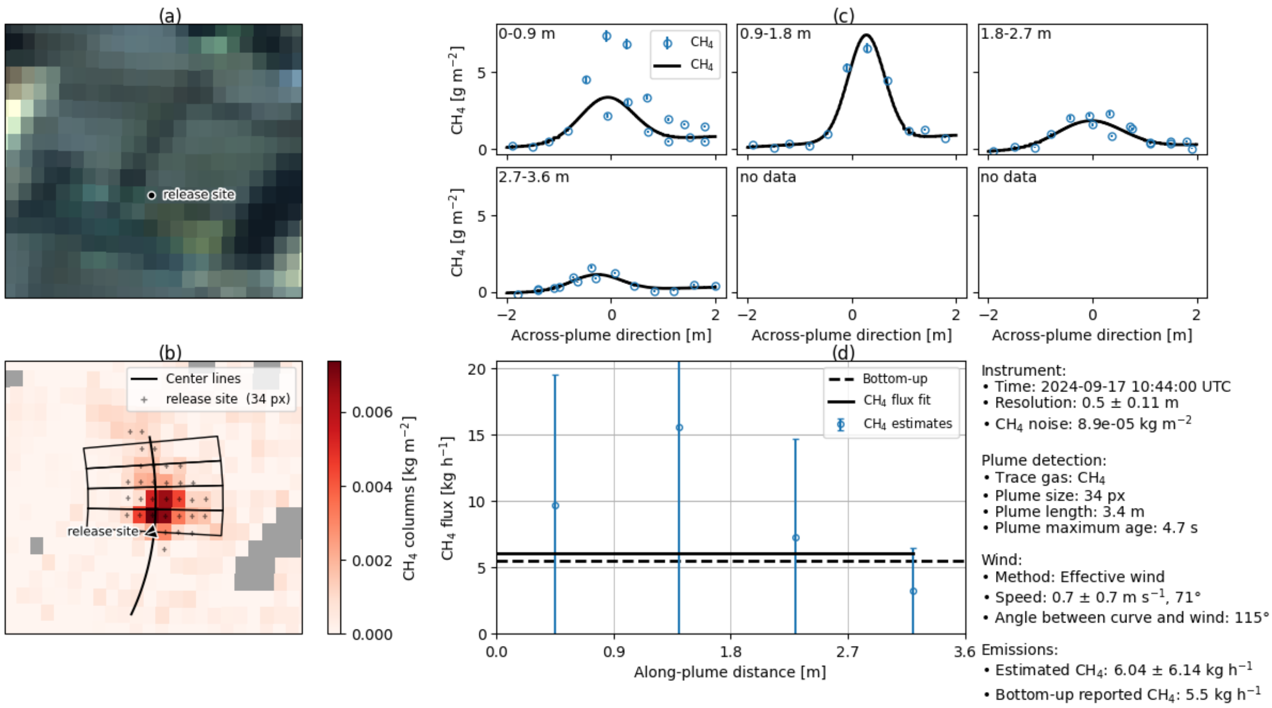

Fig. S26: M015_240917_FRA_Pau_Methane_4200ft_Line_10001_124339_000_rdn_csf_results

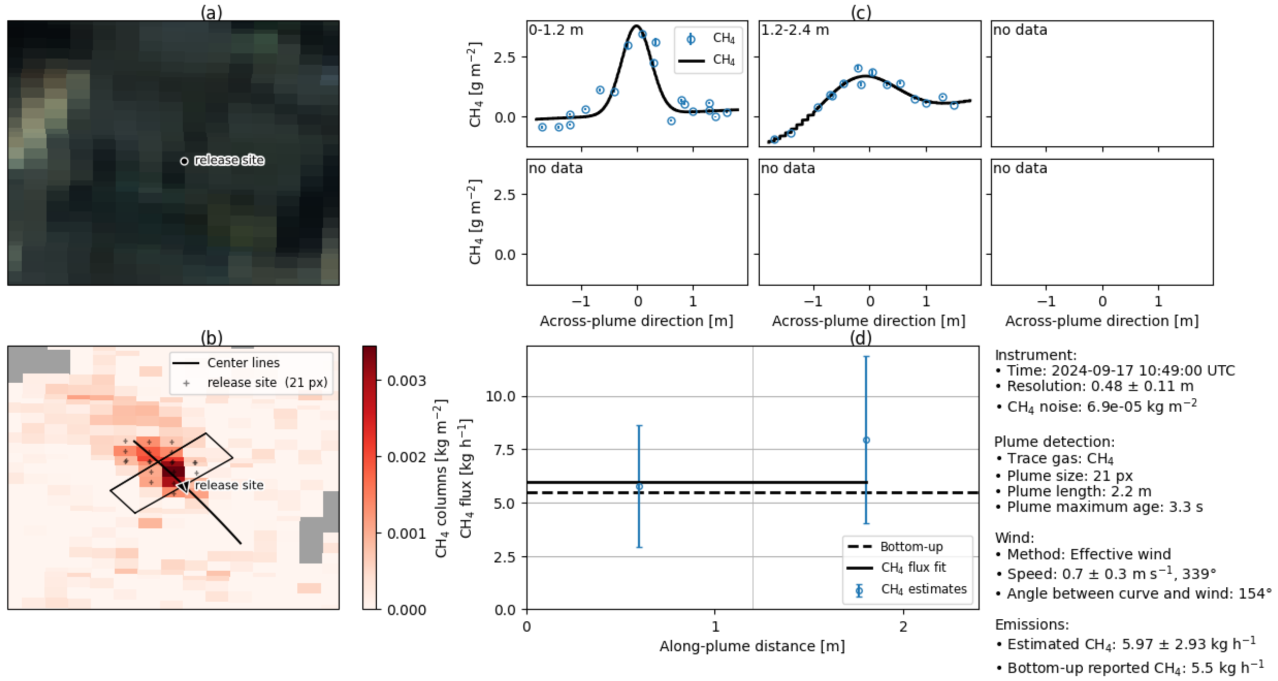

Fig. S27: M015_240917_FRA_Pau_Methane_4200ft_Line_20001_124929_000_rdn_csf_results

Day 3: 18.09.2024

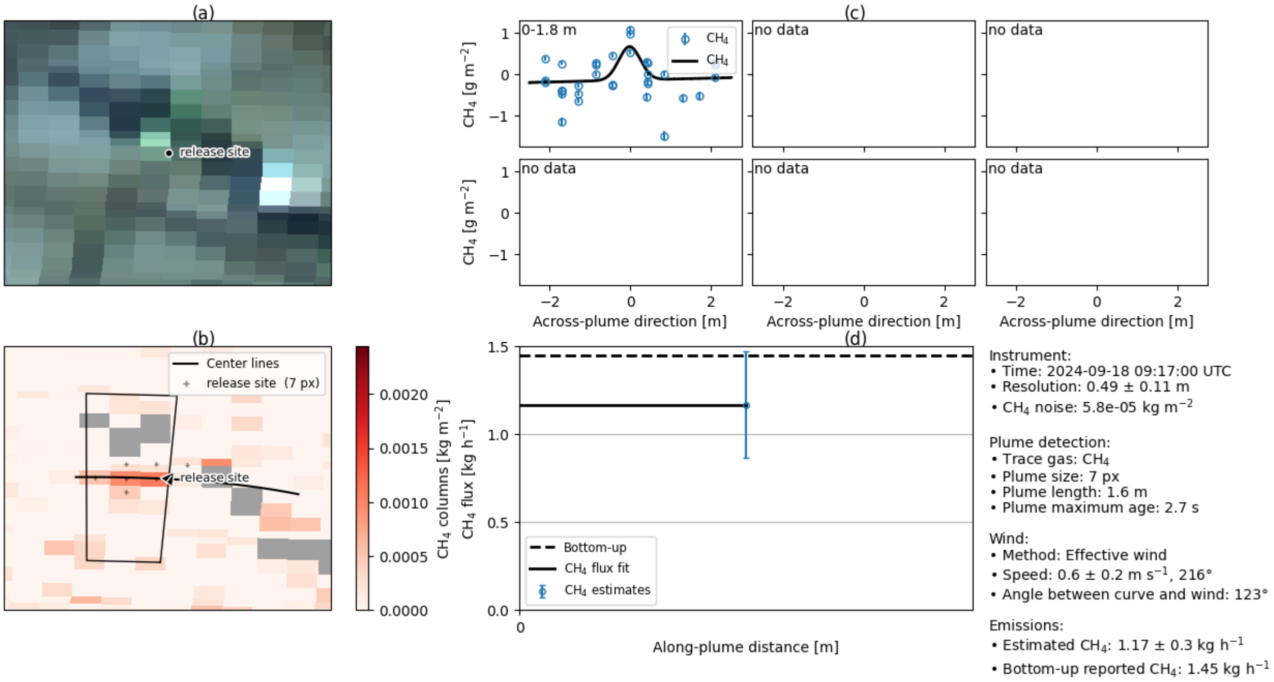

Fig. S28: M016_240918_FRA_Pau_Methane_4200ft_Line_20001_111708_000_rdn_csf_results

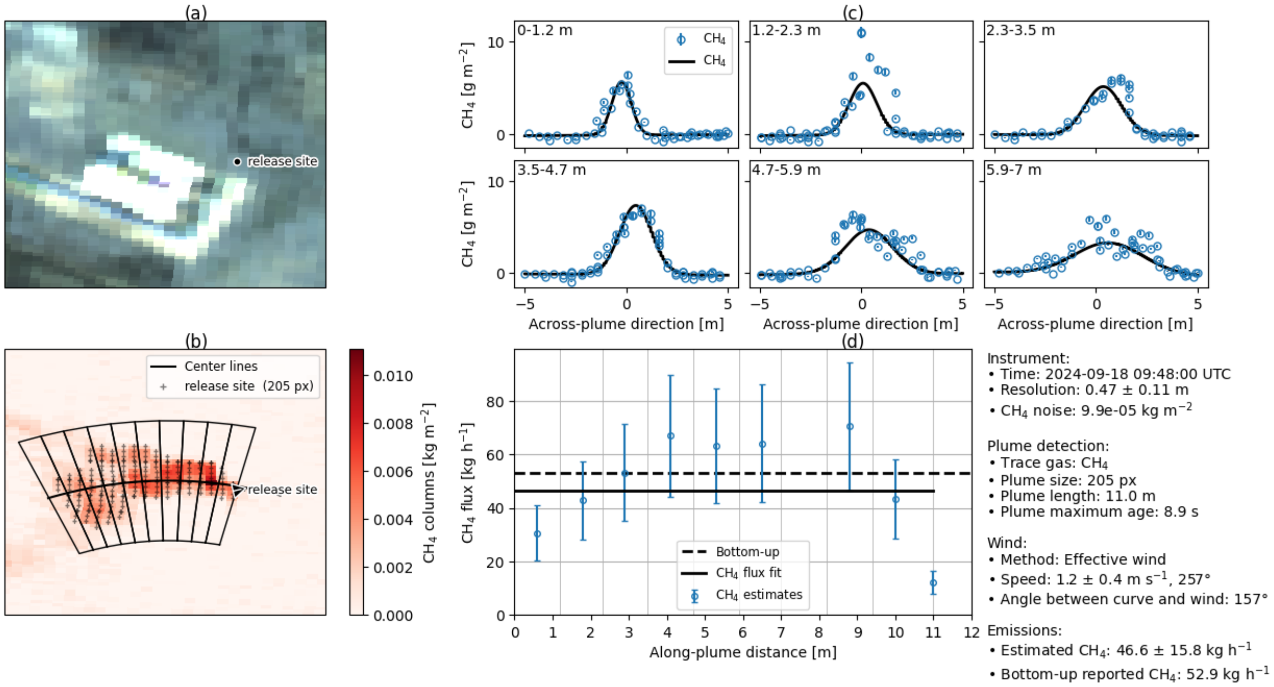

Fig. S29: M016_240918_FRA_Pau_Methane_4200ft_Line_20001_114730_000_rdn_csf_results

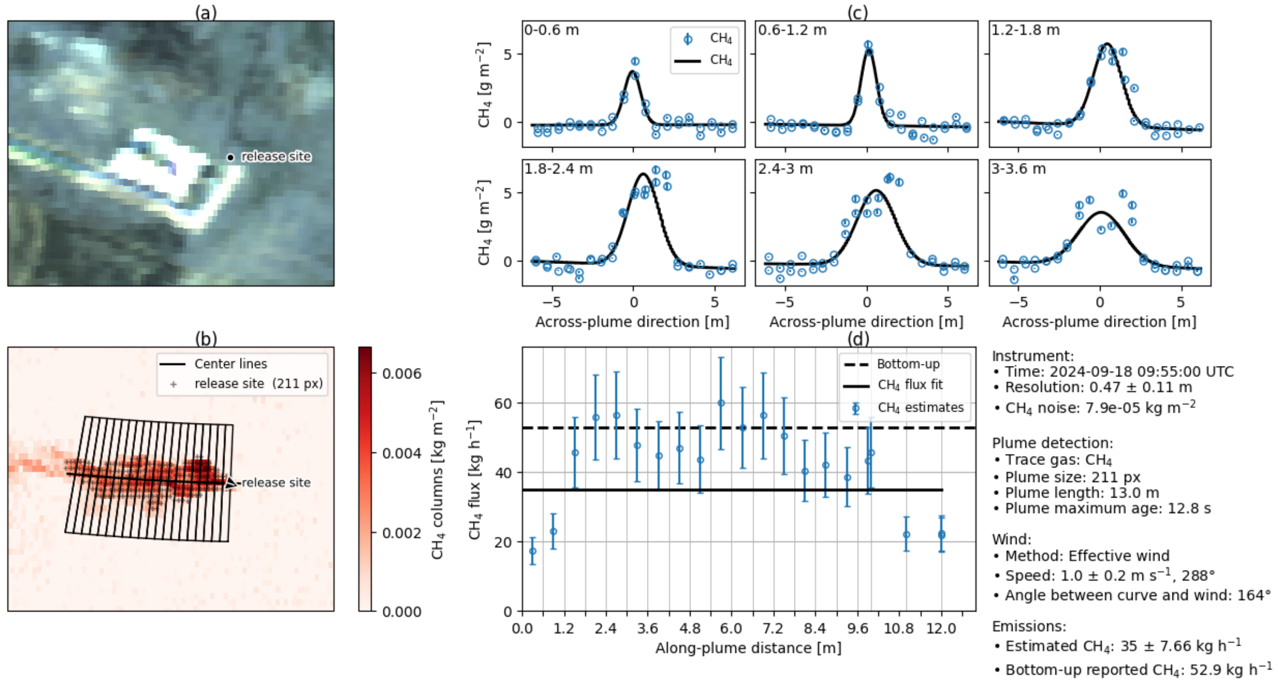

Fig. S30: M016_240918_FRA_Pau_Methane_4200ft_Line_10001_115436_000_rdn_csf_results

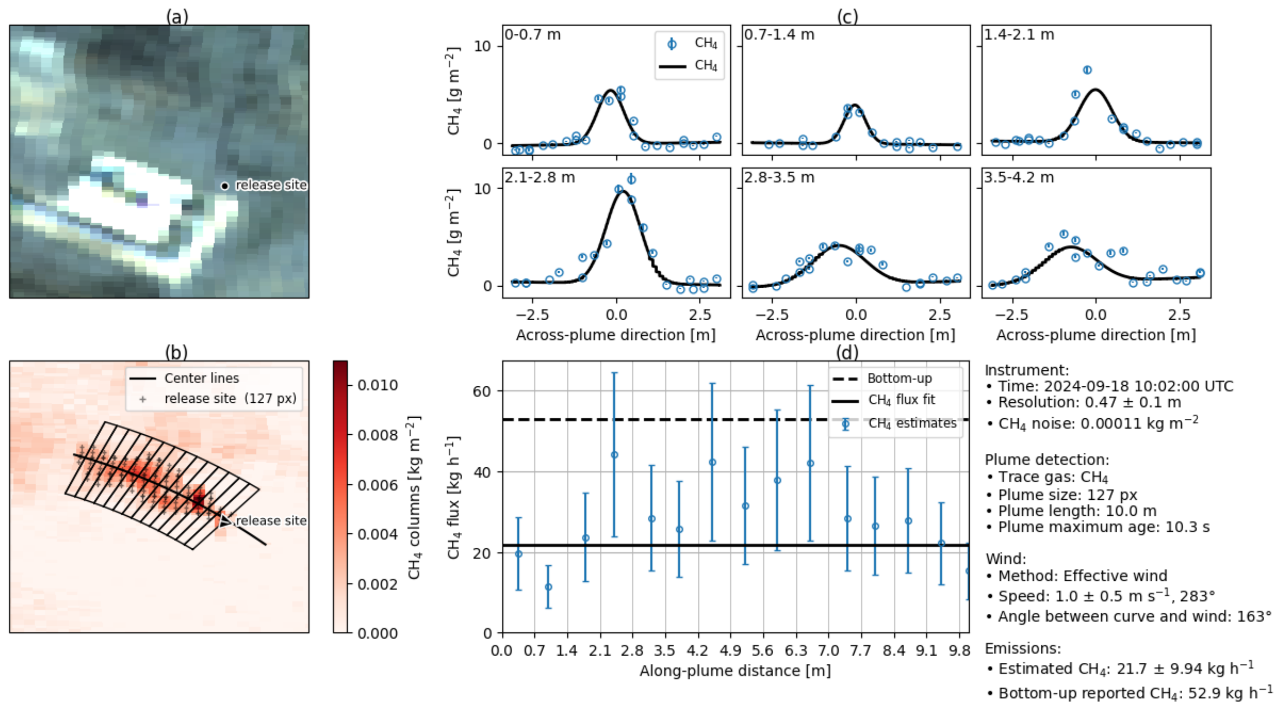

Fig. S31: M016_240918_FRA_Pau_Methane_4200ft_Line_20001_120152_000_rdn_csf_results

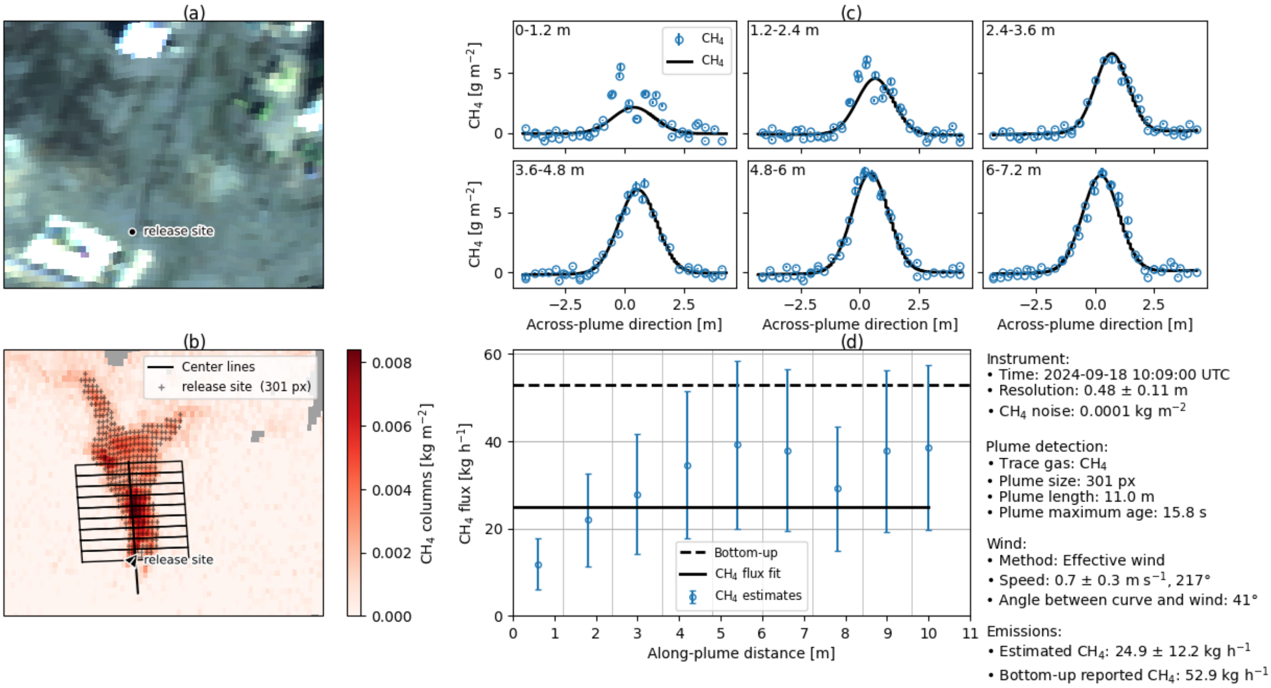

Fig. S32: M016_240918_FRA_Pau_Methane_4200ft_Line_10001_120855_000_rdn_csf_results

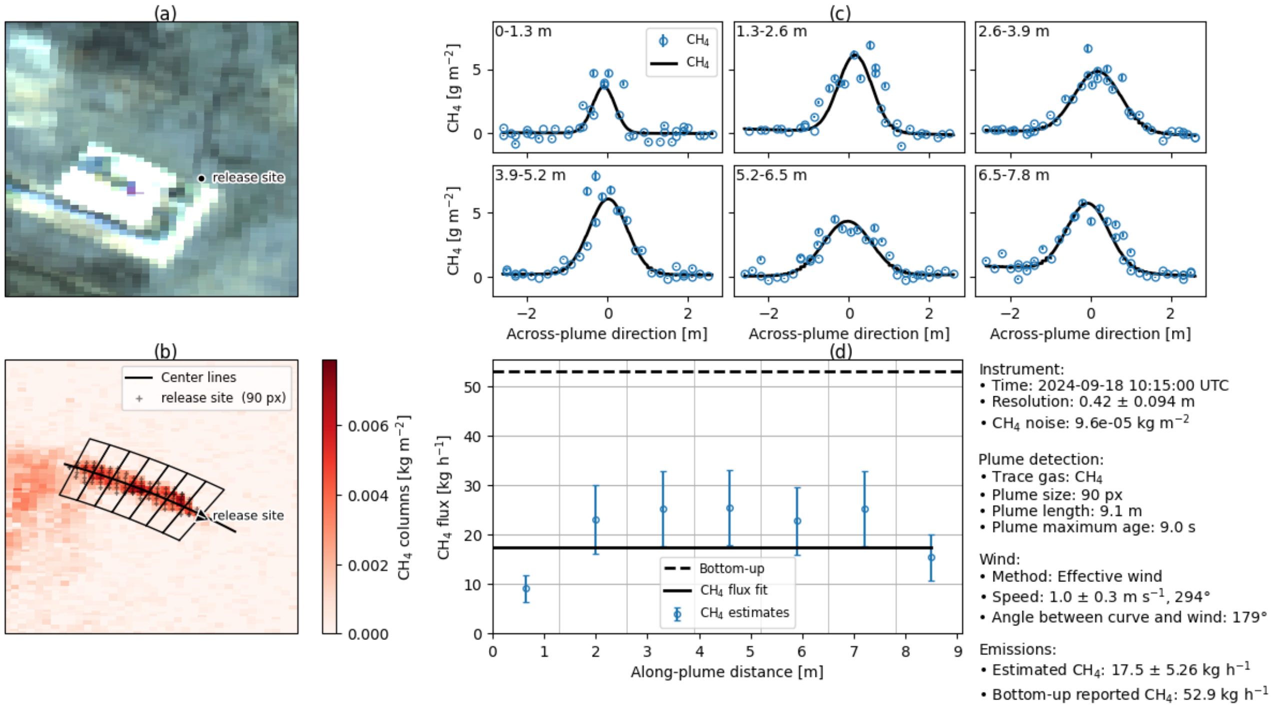

Fig. S33: M016_240918_FRA_Pau_Methane_3000ft_Line_20001_121435_000_rdn_csf_results

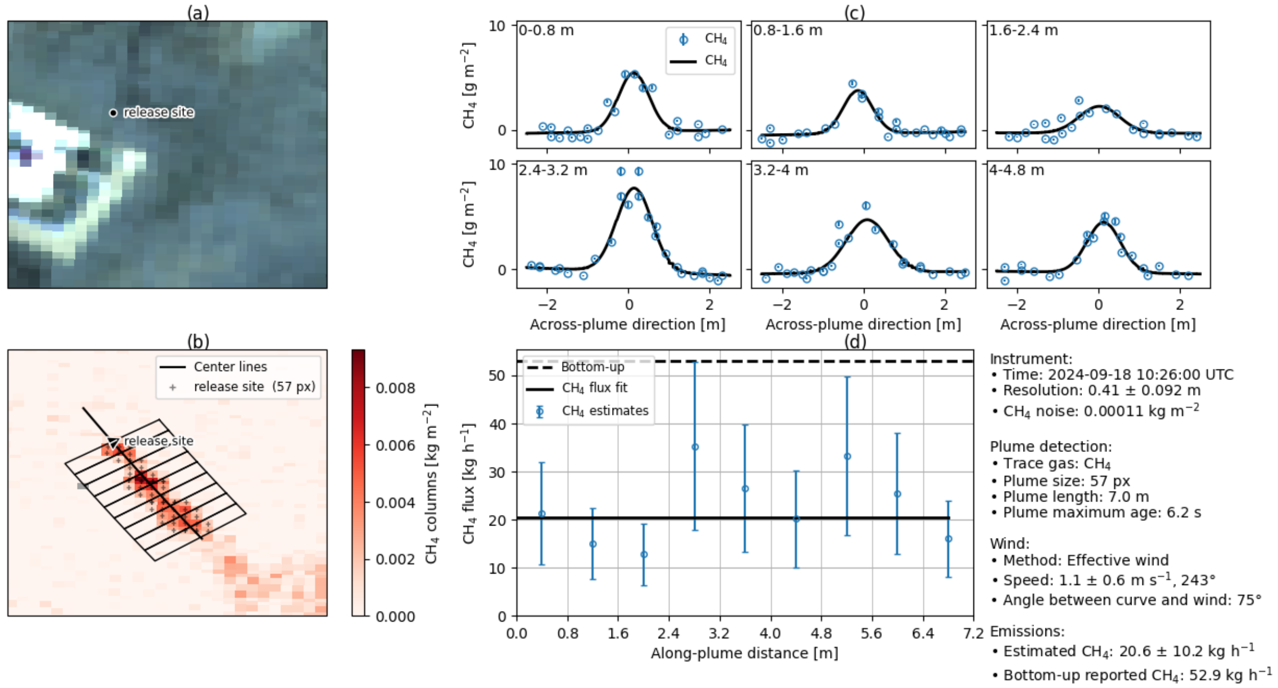

Fig. S34: M016_240918_FRA_Pau_Methane_3000ft_Line_20001_122622_000_rdn_csf_results

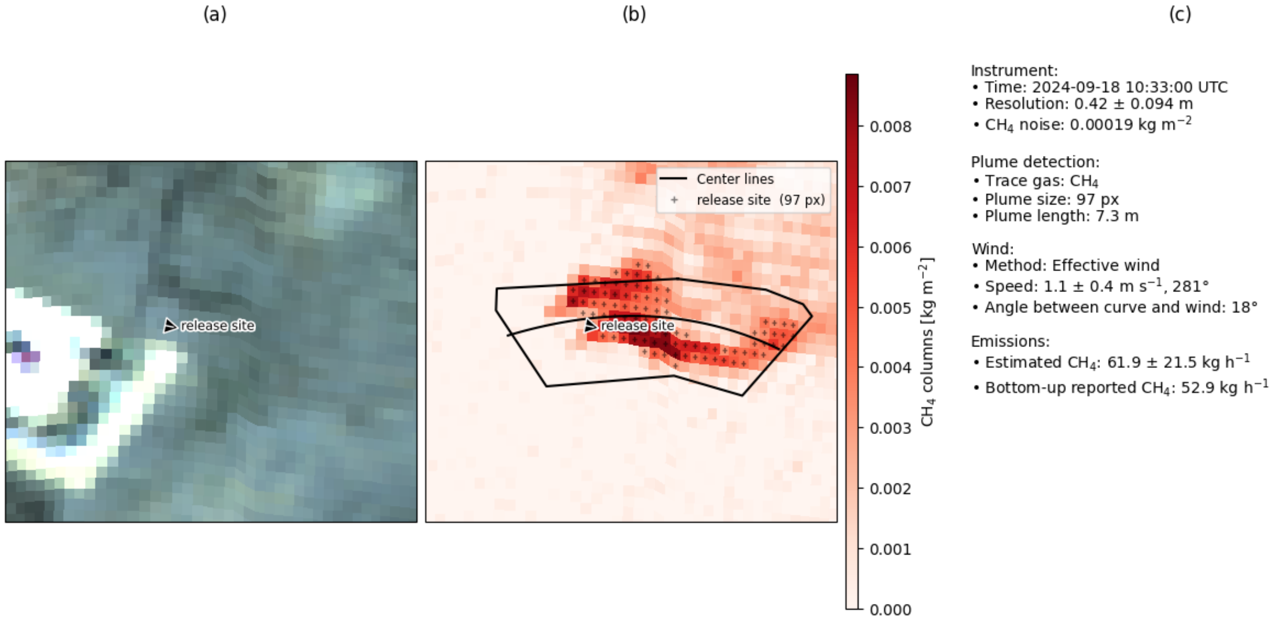

Fig. S35: M016_240918_FRA_Pau_Methane_3000ft_Line_10001_123241_000_rdn_ime_results

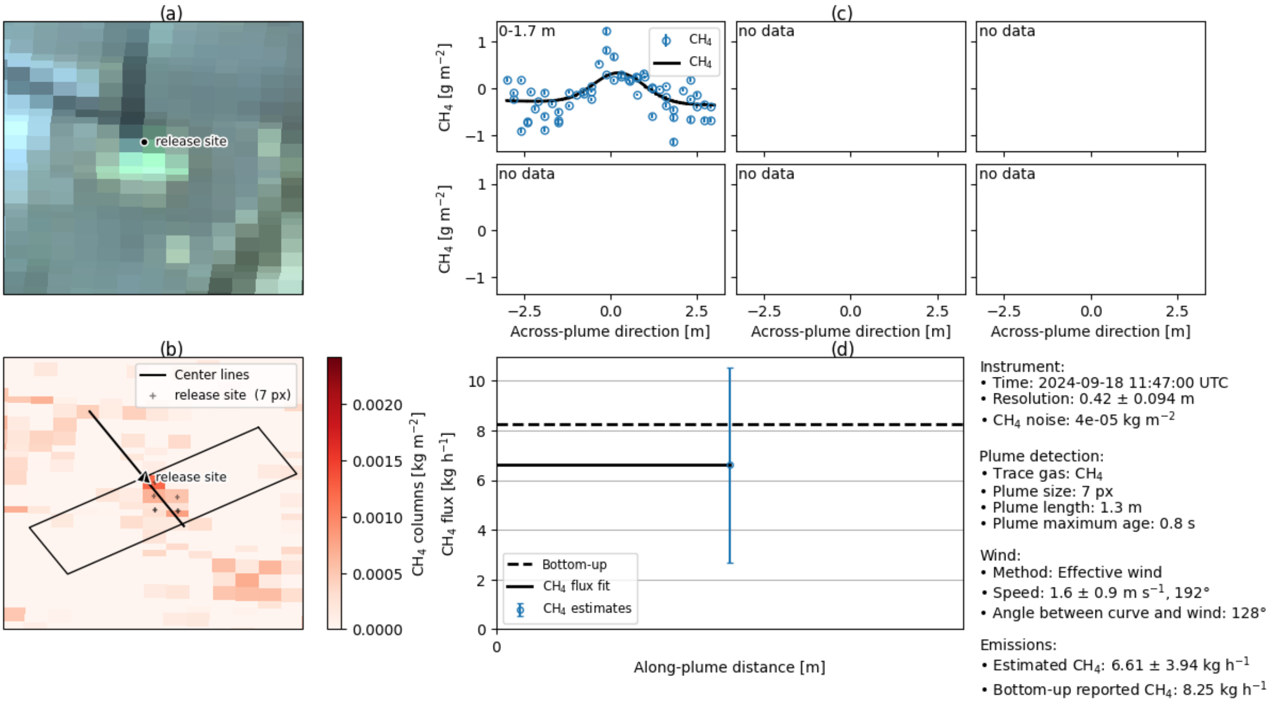

Fig. S36: M016_240918_FRA_Pau_Methane_3000ft_Line_20001_134718_000_rdn_csf_results

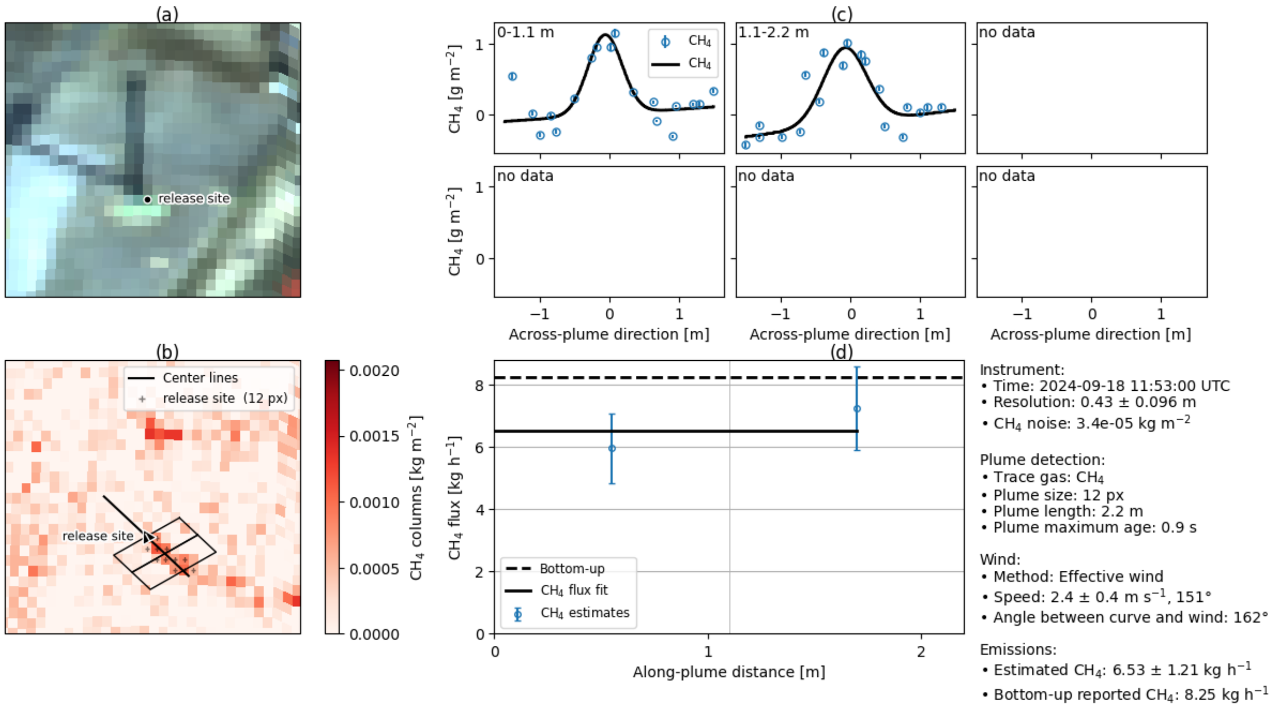

Fig. S37: M016_240918_FRA_Pau_Methane_3000ft_Line_10001_135313_000_rdn_csf_results

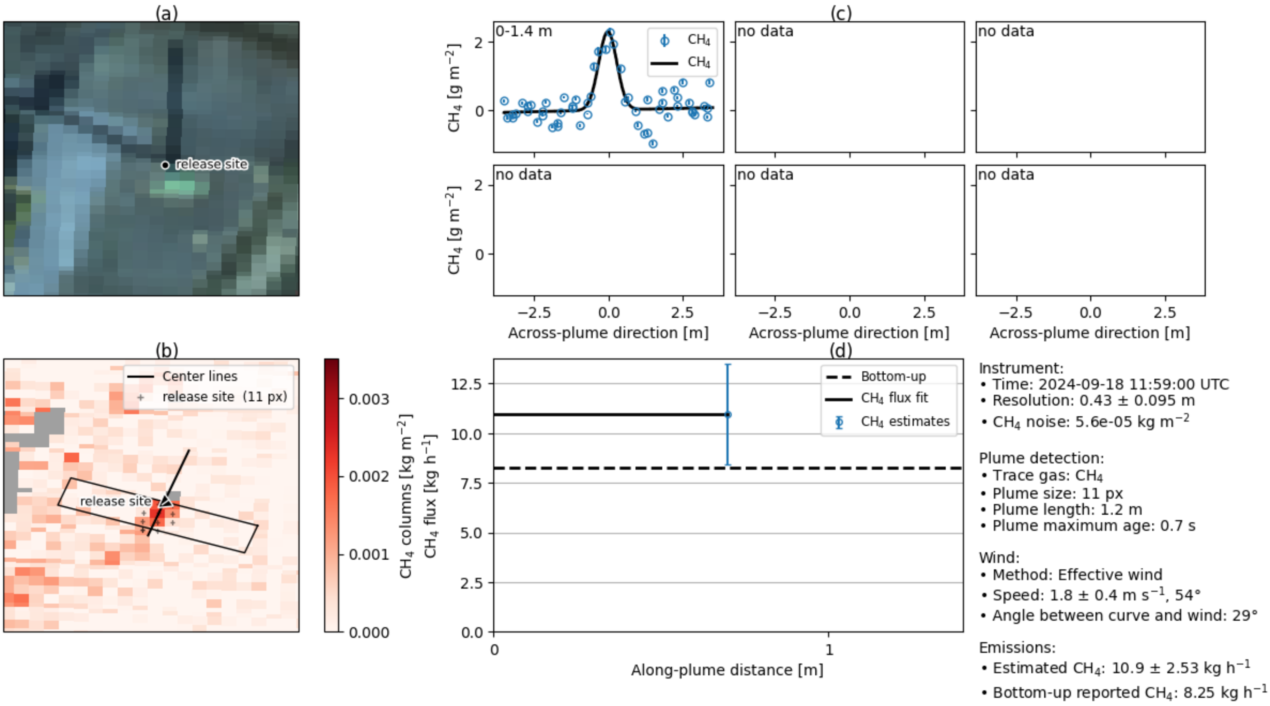

Fig. S38: M016_240918_FRA_Pau_Methane_3000ft_Line_20001_135839_000_rdn_csf_results

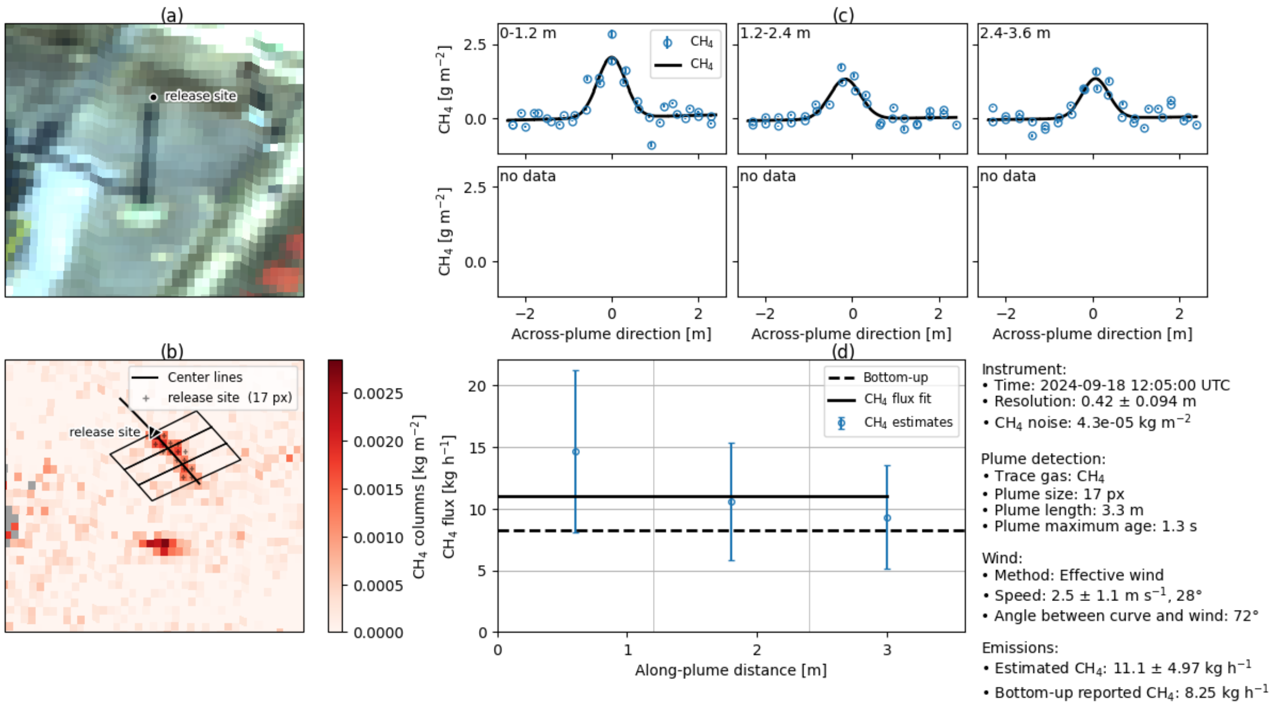

Fig. S39: M016_240918_FRA_Pau_Methane_3000ft_Line_10001_140447_000_rdn_csf_results

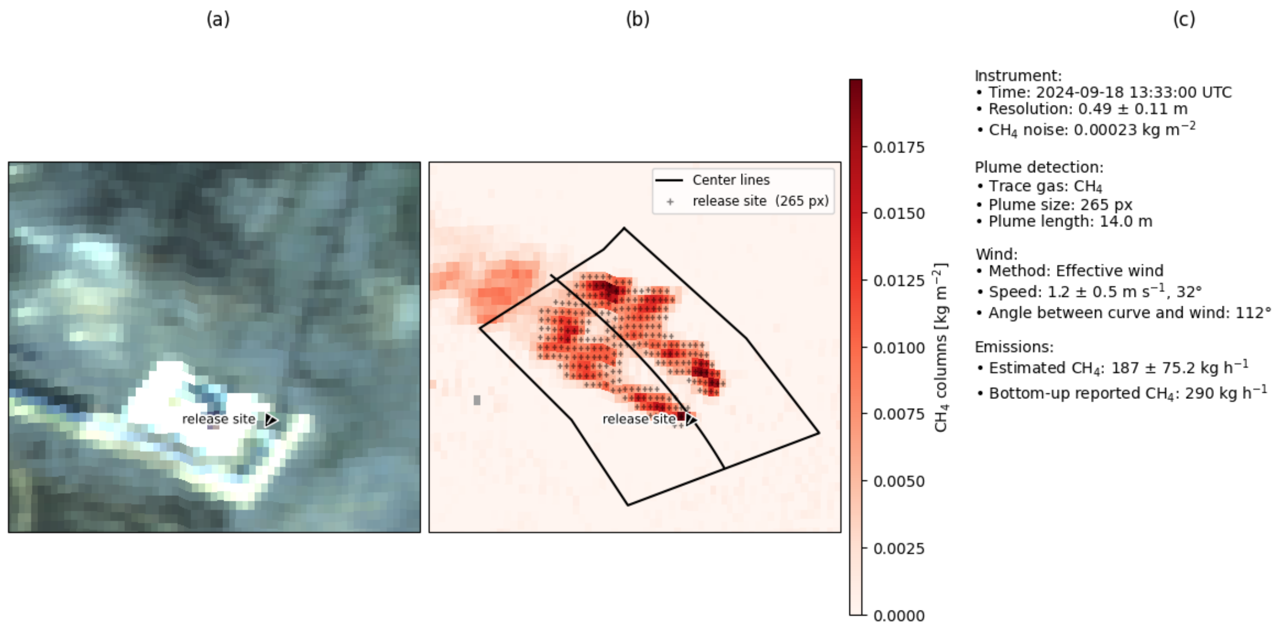

Fig. S40: M016_240918_FRA_Pau_Methane_4200ft_Line_10001_153306_000_rdn_ime_results

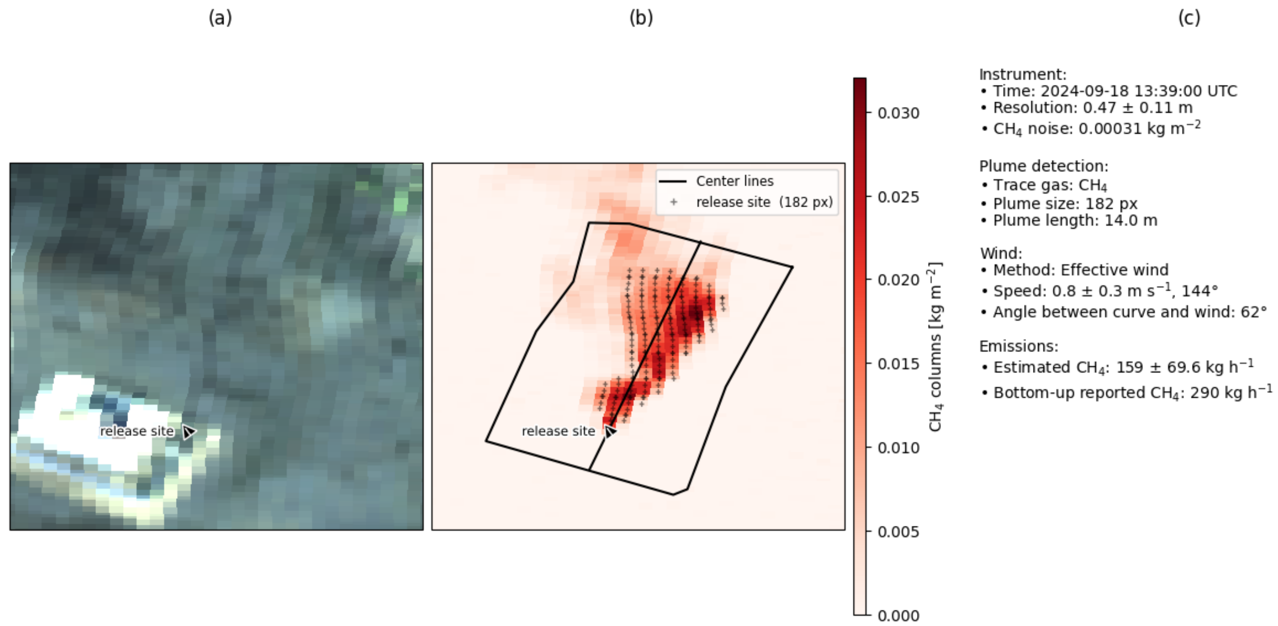

Fig. S41: M016_240918_FRA_Pau_Methane_4200ft_Line_20001_153853_000_rdn_ime_results

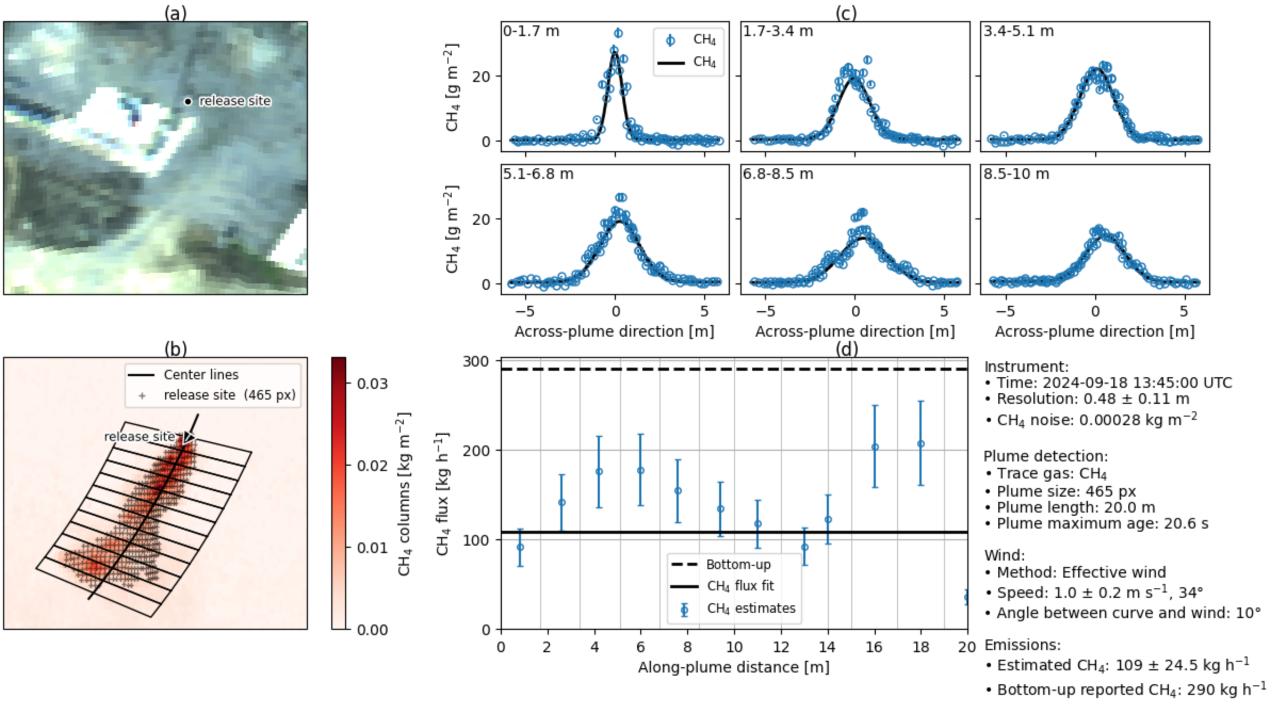

Fig. S42: M016_240918_FRA_Pau_Methane_4200ft_Line_10001_154503_000_rdn_csf_results

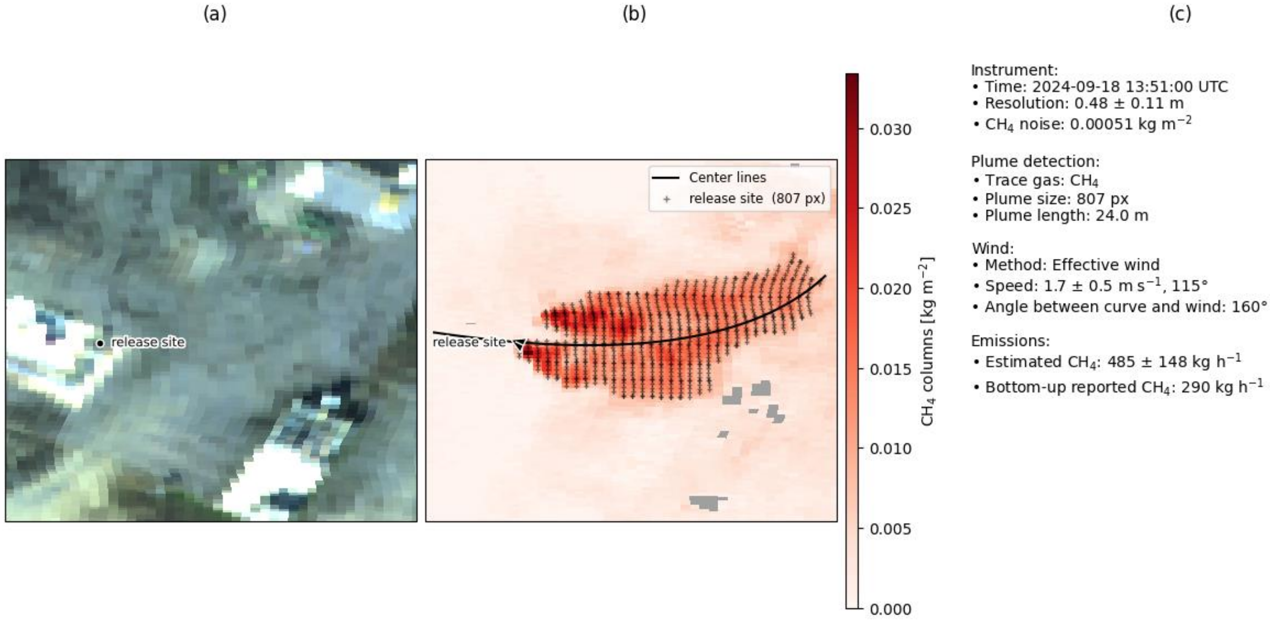

Fig. S43: M016_240918_FRA_Pau_Methane_4200ft_Line_20001_155035_000_rdn_ime_results

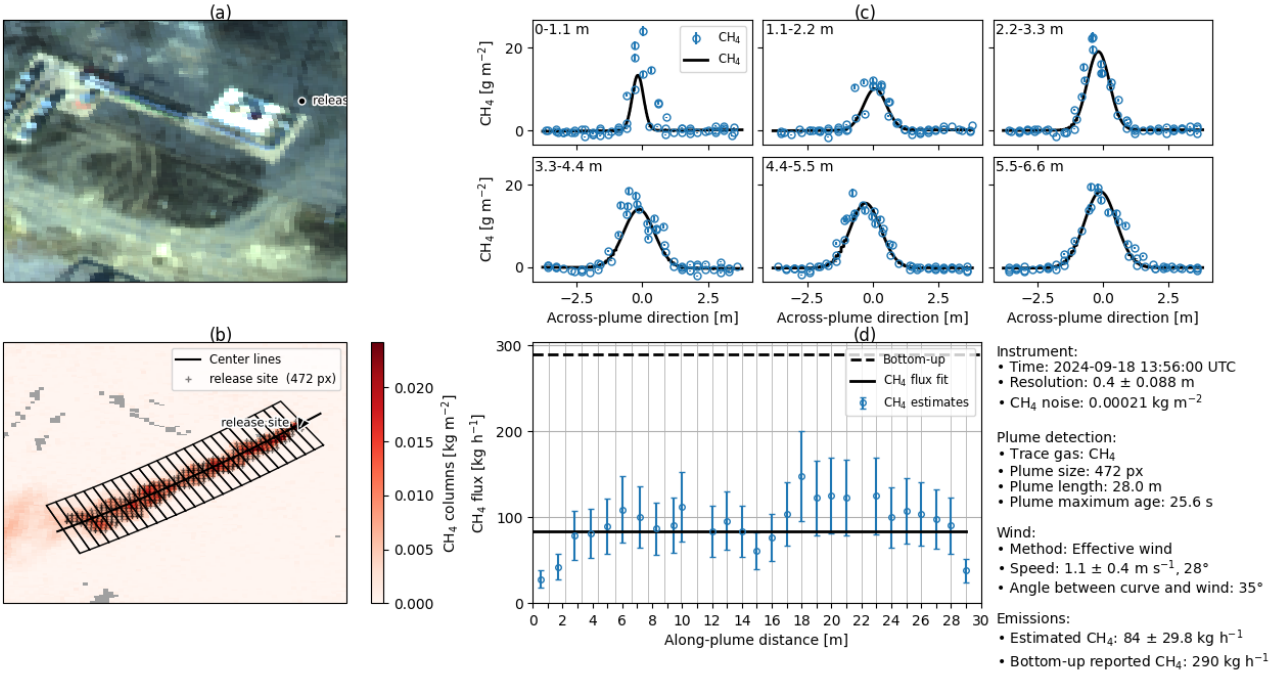

Fig. S44: M016_240918_FRA_Pau_Methane_3000ft_Line_20001_155622_000_rdn_csf_results

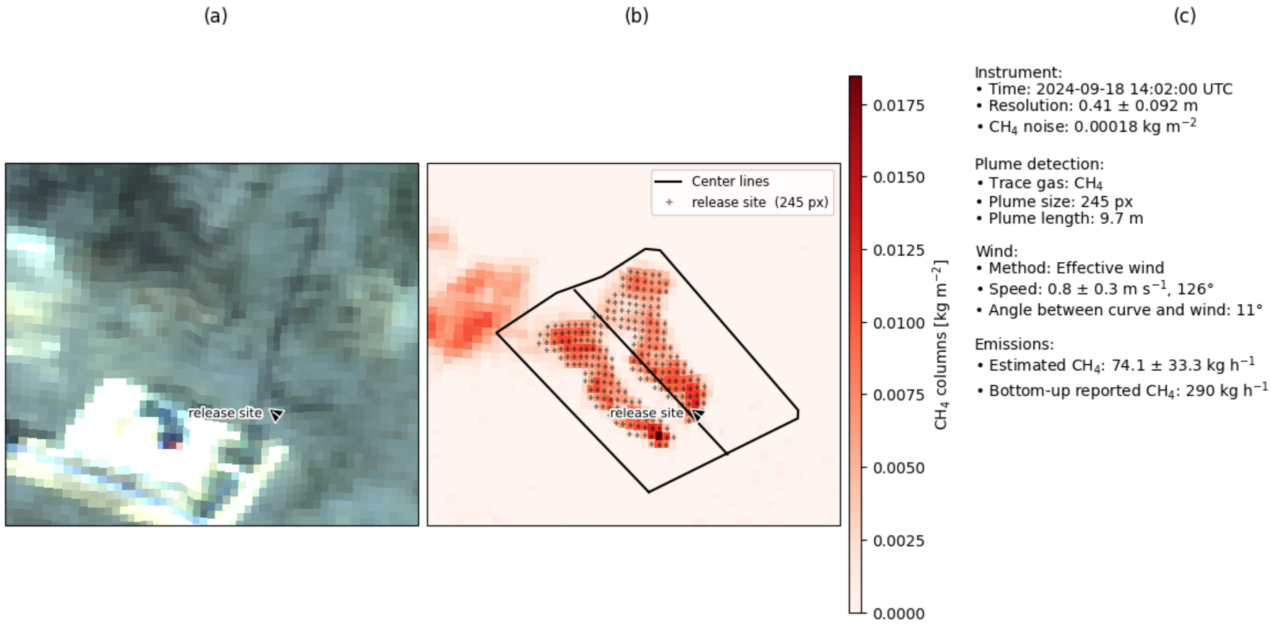

Fig. S45: M016_240918_FRA_Pau_Methane_3000ft_Line_10001_160215_000_rdn_ime_results

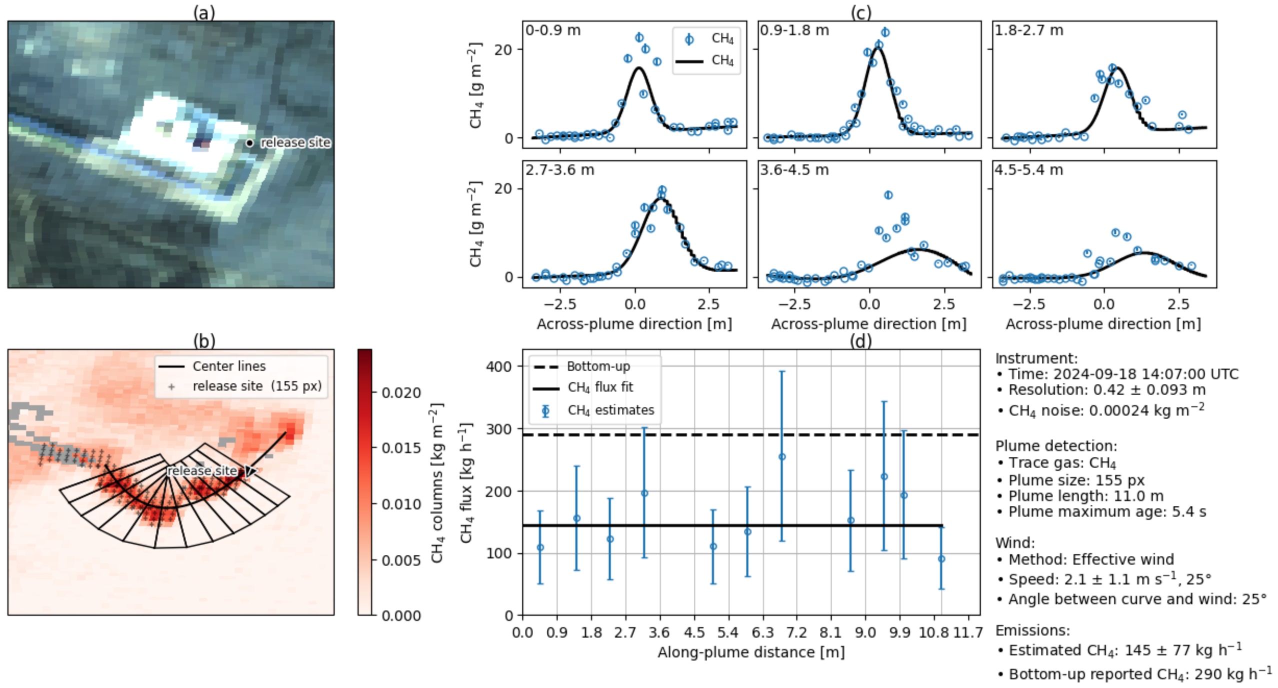

Fig. S46: M016_240918_FRA_Pau_Methane_3000ft_Line_20001_160728_000_rdn_csf_results

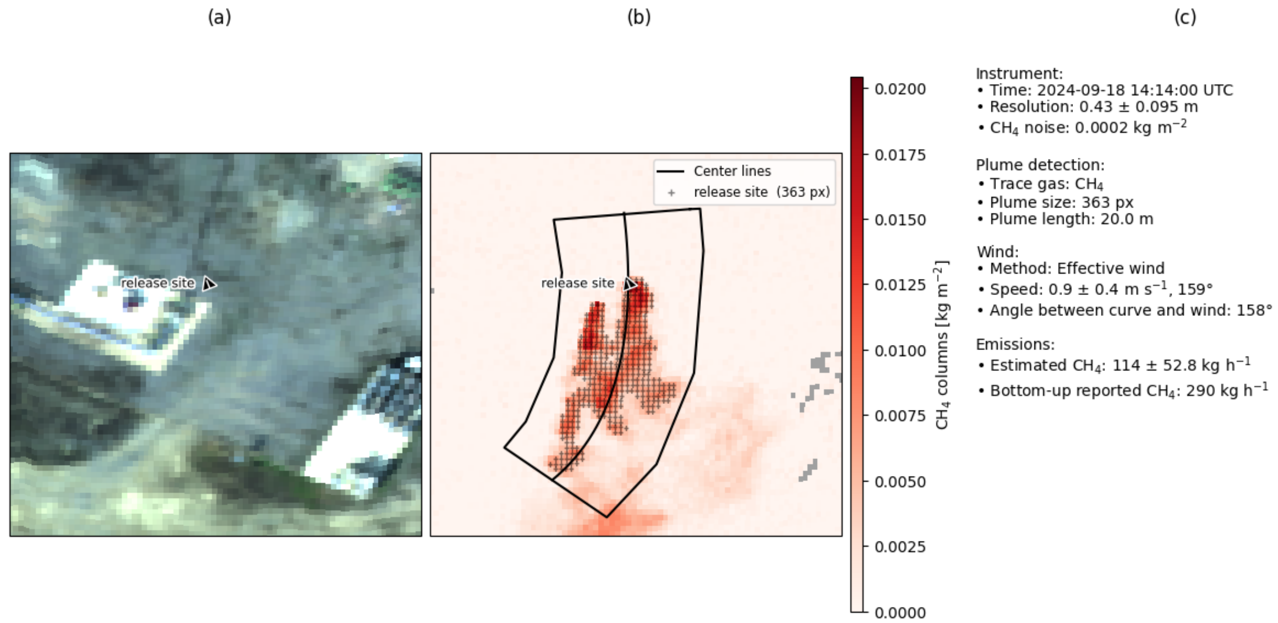

Fig. S47: M016_240918_FRA_Pau_Methane_3000ft_Line_10001_161350_000_rdn_ime_results

Day 4: 19.09.2024

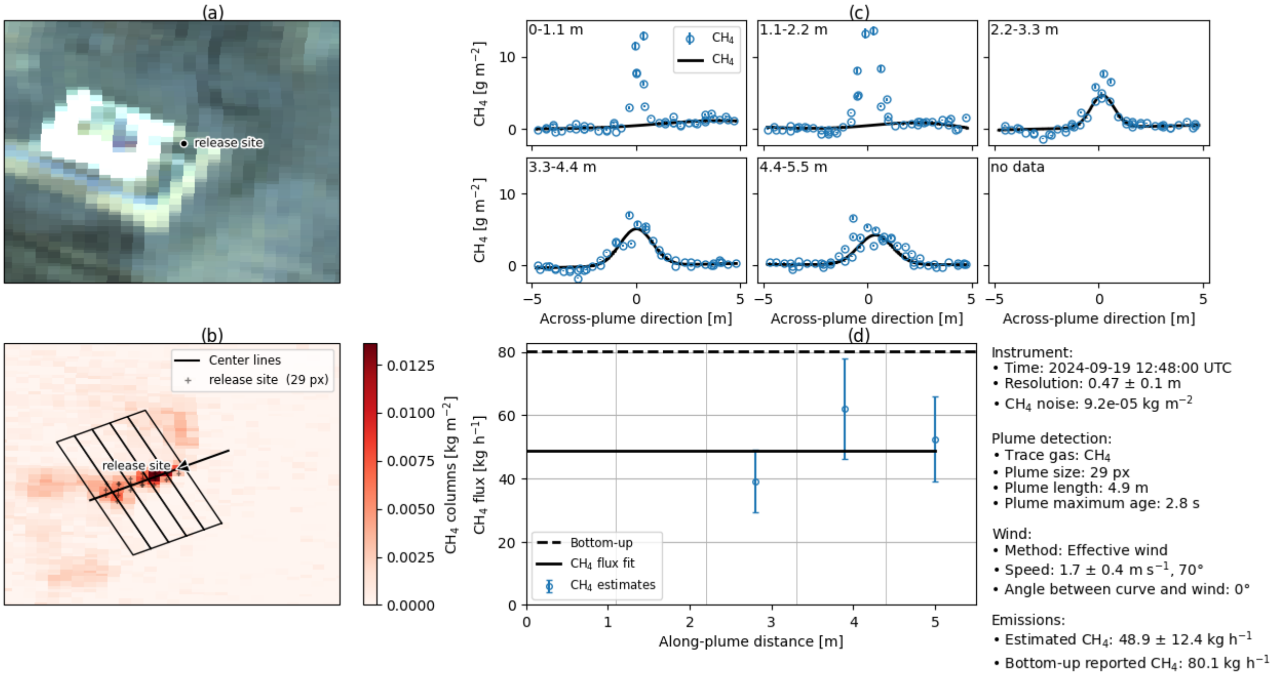

Fig. S48: M017_240919_FRA_Pau_Methane_4200ft_Line_20001_144745_000_rdn_csf_results

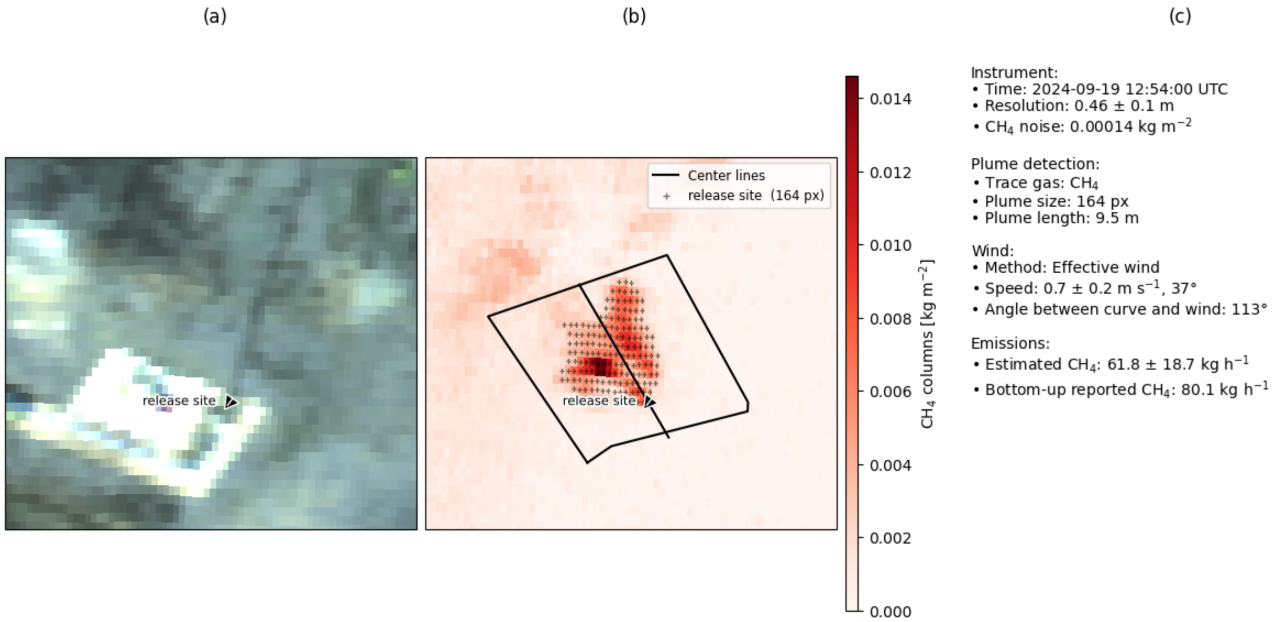

Fig. S49: M017_240919_FRA_Pau_Methane_4200ft_Line_10001_145410_000_rdn_ime_results

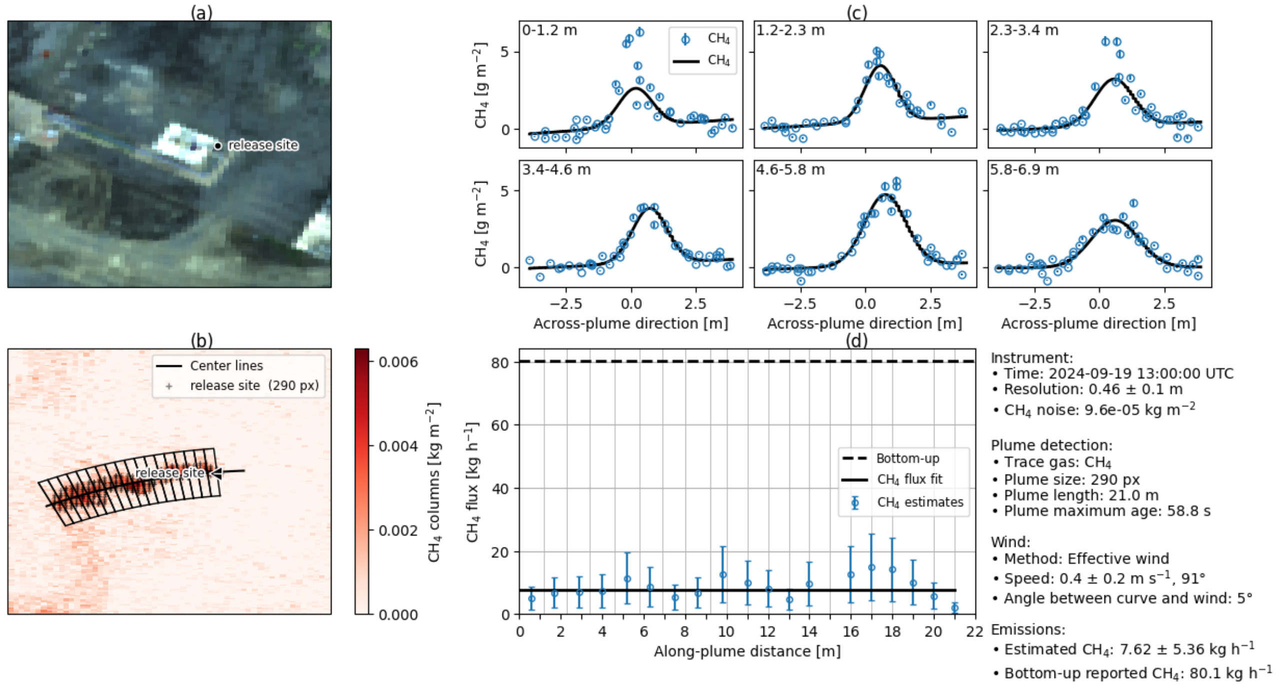

Fig. S50: M017_240919_FRA_Pau_Methane_4200ft_Line_20001_150007_000_rdn_csf_results

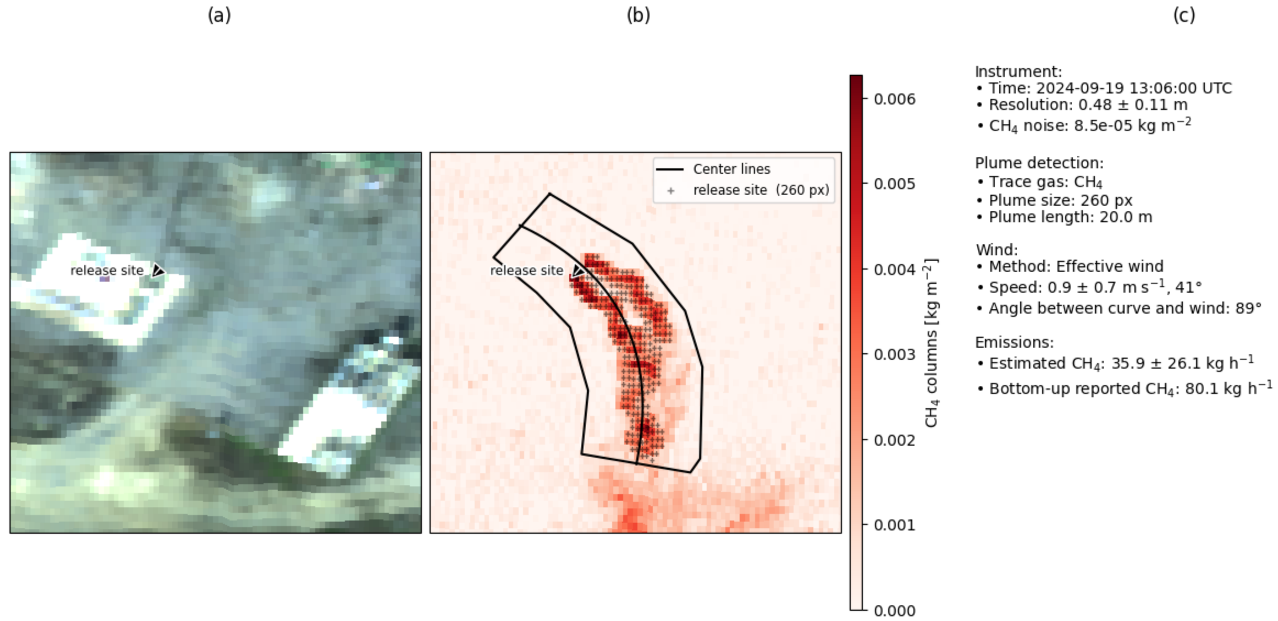

Fig. S51: M017_240919_FRA_Pau_Methane_4200ft_Line_10001_150548_000_rdn_ime_results

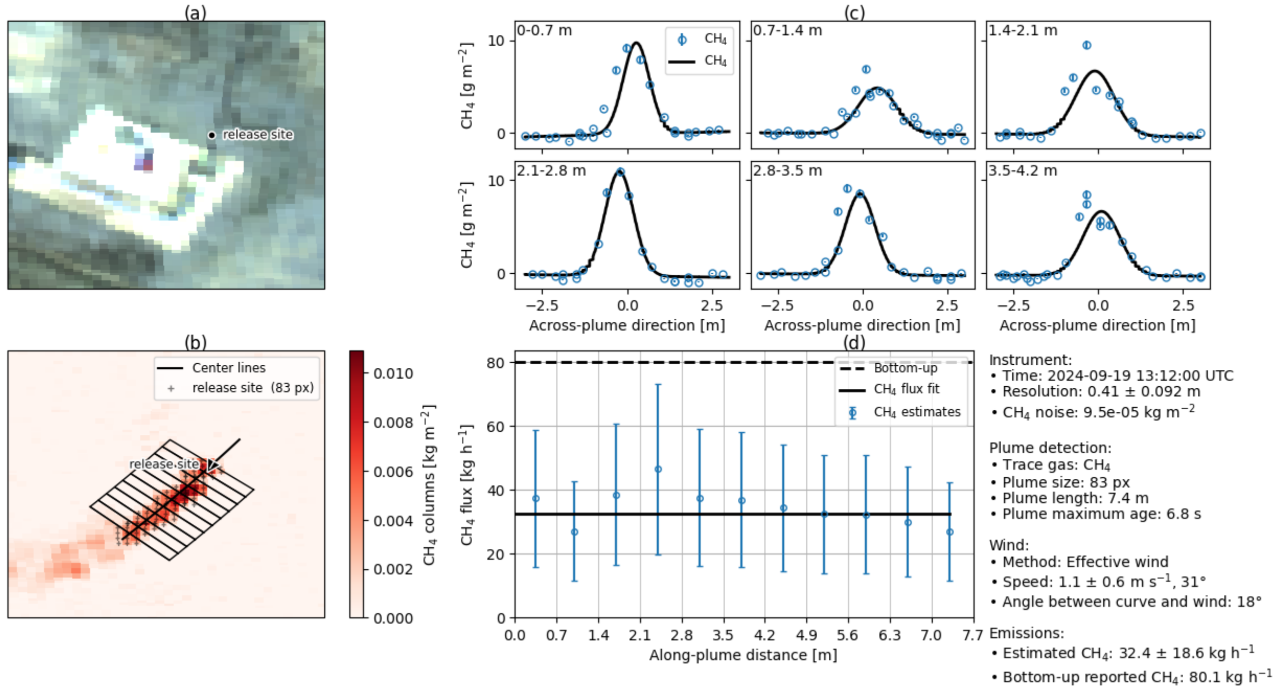

Fig. S52: M017_240919_FRA_Pau_Methane_3000ft_Line_20001_151134_000_rdn_csf_results

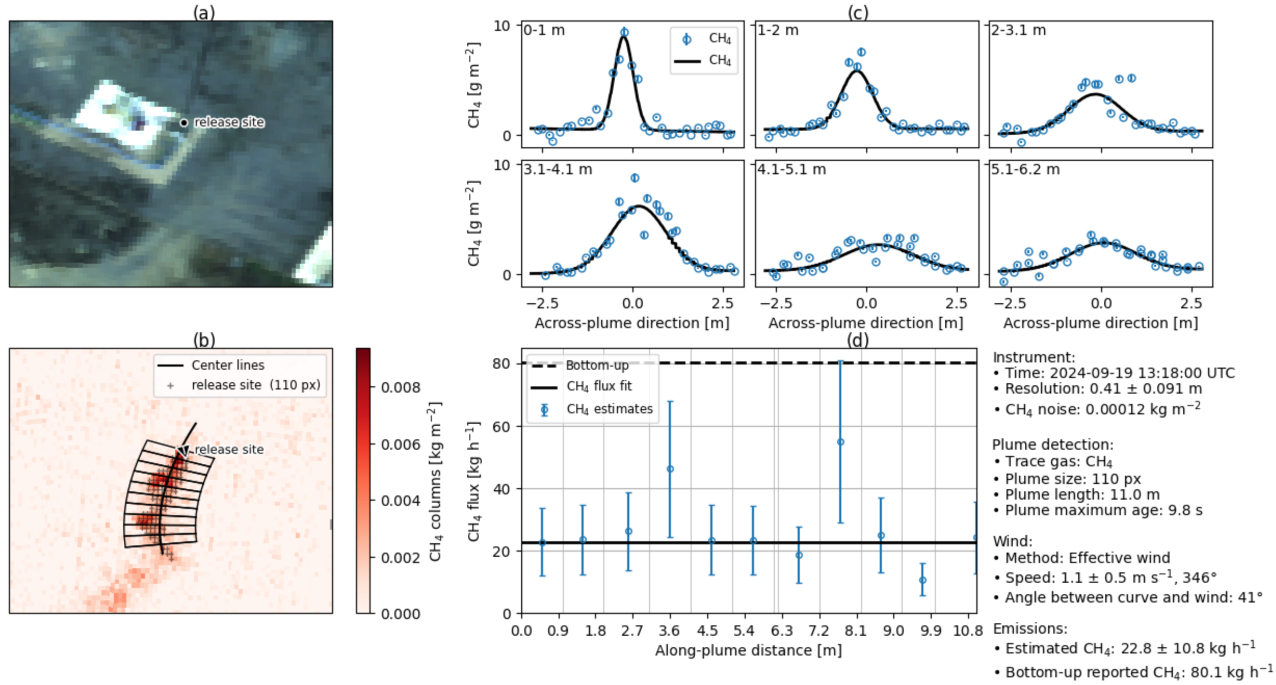

Fig. S53: M017_240919_FRA_Pau_Methane_3000ft_Line_10001_151806_000_rdn_csf_results

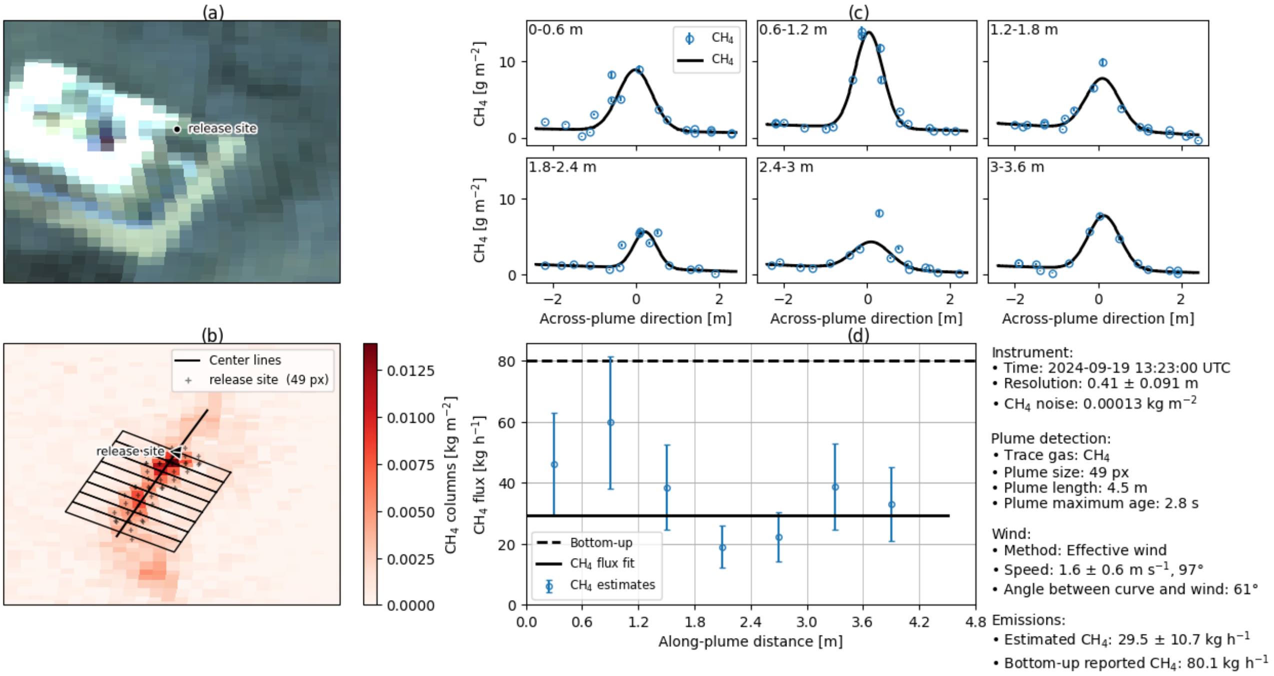

Fig. S54: M017_240919_FRA_Pau_Methane_3000ft_Line_20001_152325_000_rdn_csf_results

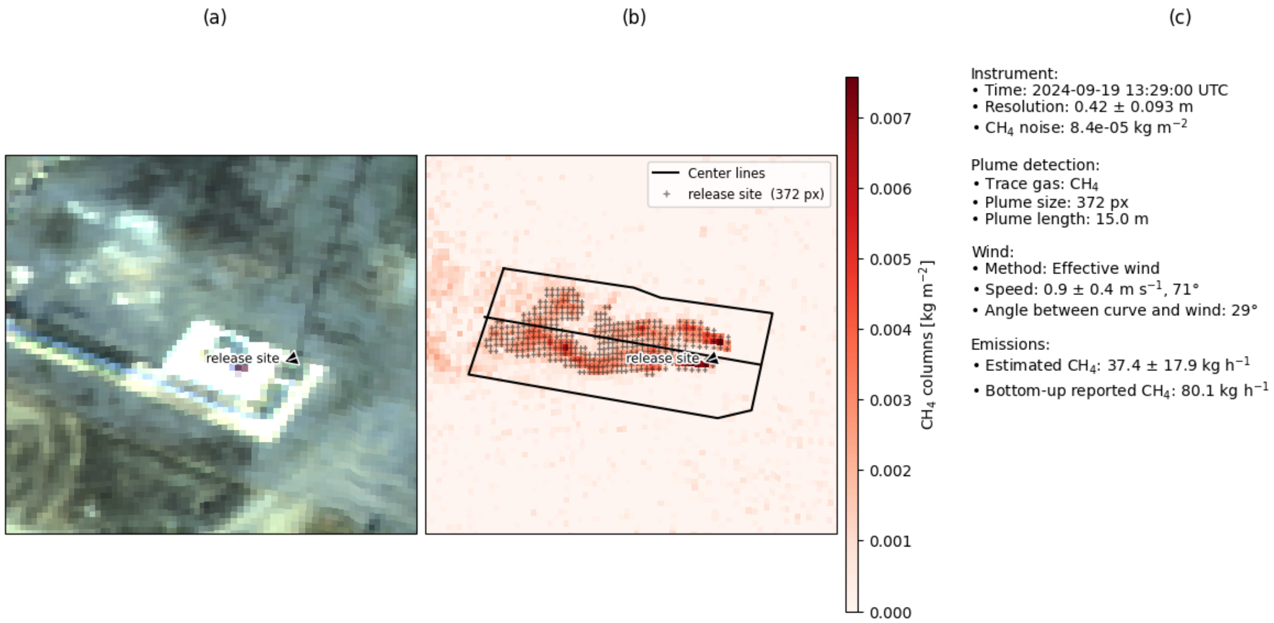

Fig. S55: M017_240919_FRA_Pau_Methane_3000ft_Line_10001_152929_000_rdn_ime_results

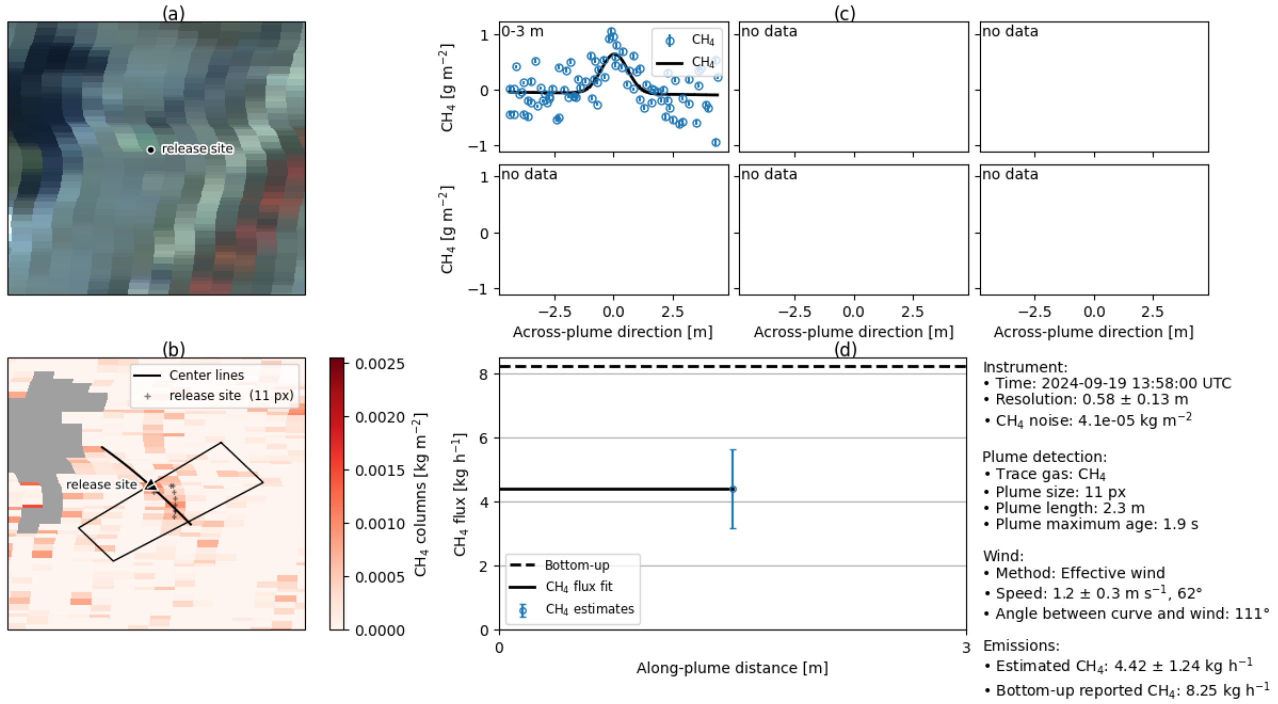

Fig. S56: M017_240919_FRA_Pau_Methane_6000ft_Line_10001_155818_000_rdn_csf_results

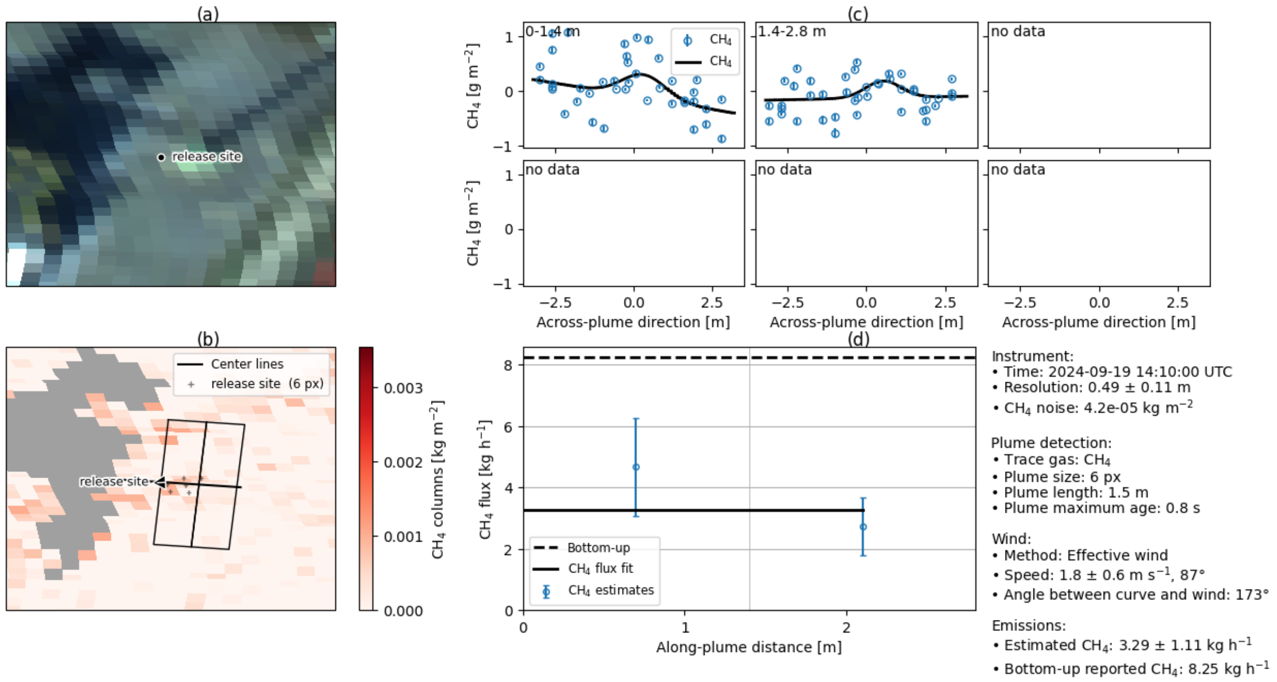

Fig. S57: M017_240919_FRA_Pau_Methane_4200ft_Line_20001_160932_000_rdn_csf_results

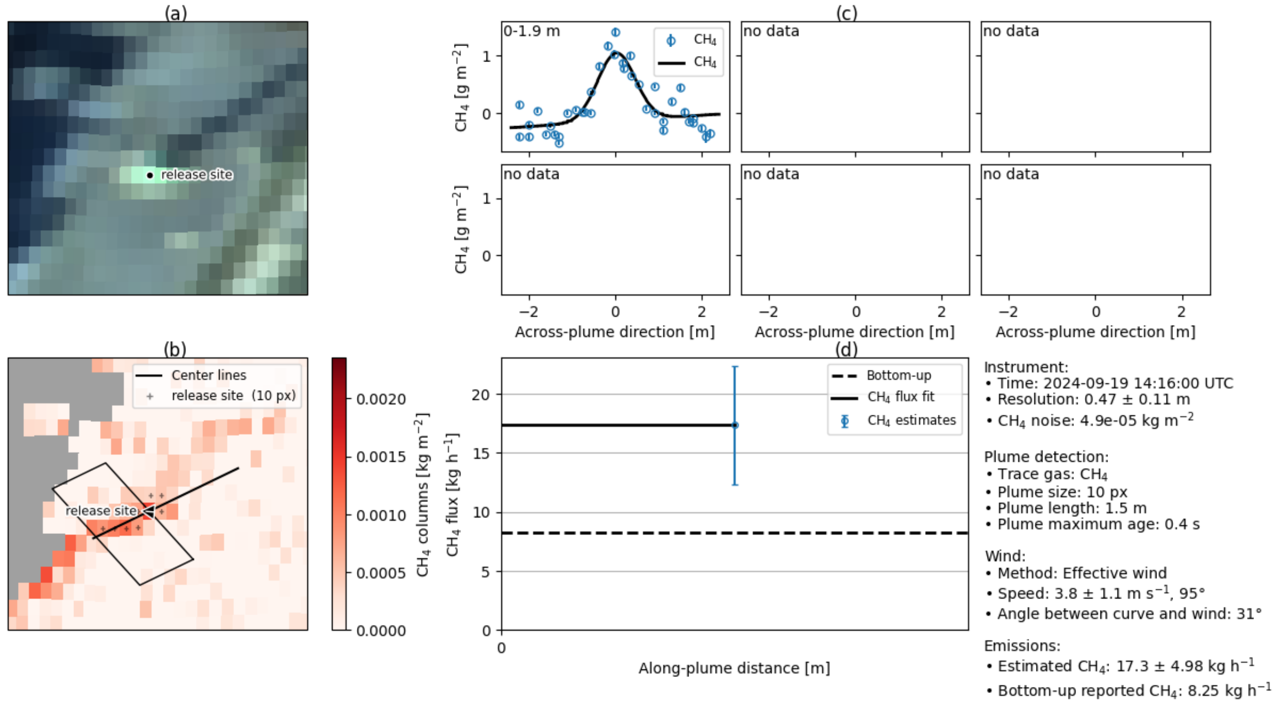

Fig. S58: M017_240919_FRA_Pau_Methane_4200ft_Line_10001_161600_000_rdn_csf_results

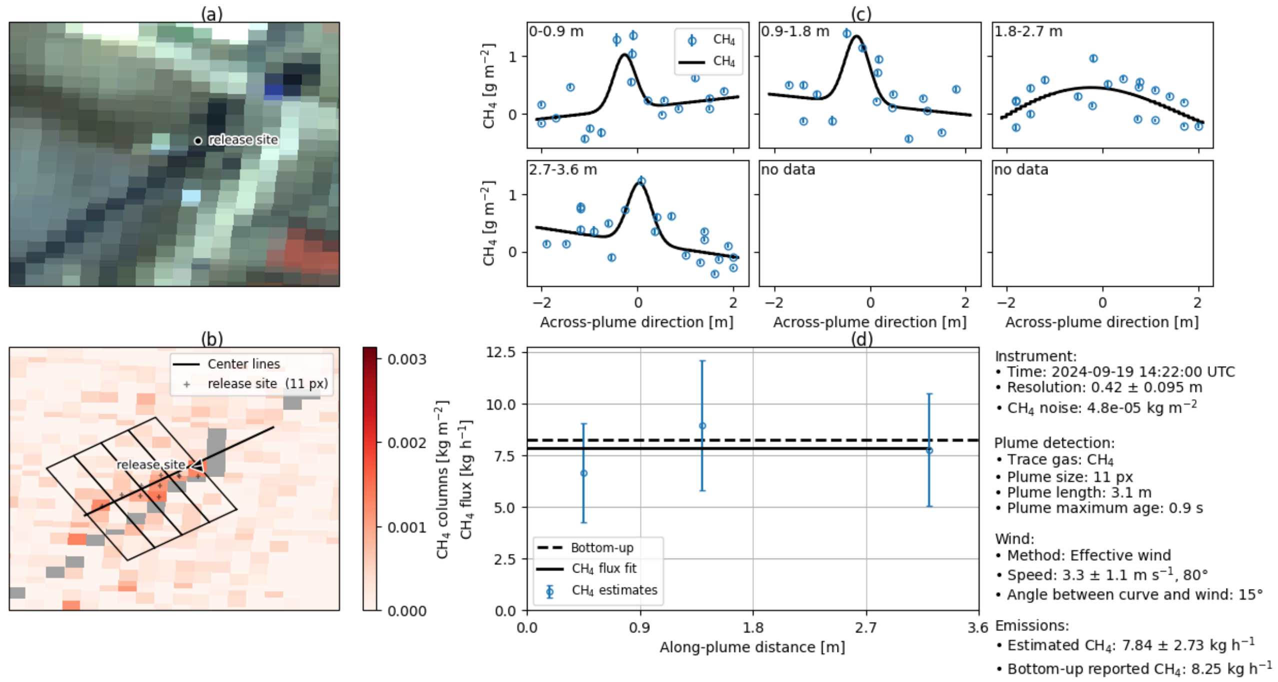

Fig. S59: M017_240919_FRA_Pau_Methane_3000ft_Line_20001_162135_000_rdn_csf_results

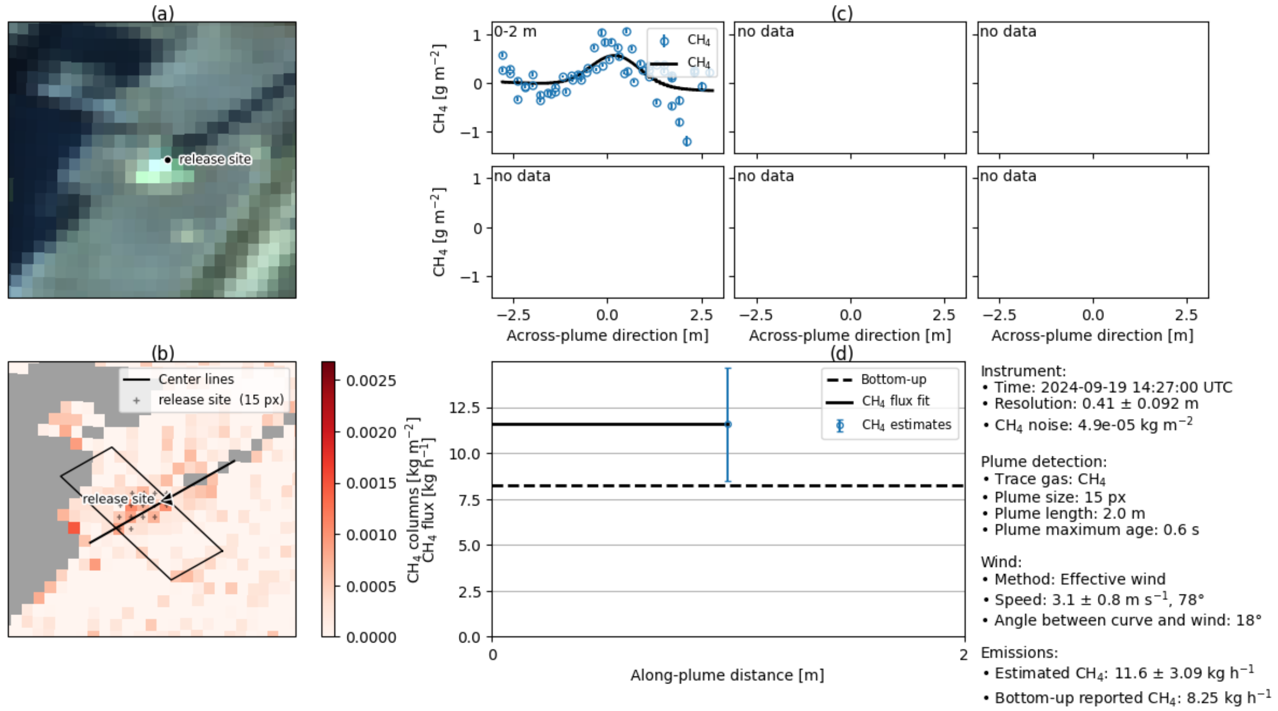

Fig. S60: M017_240919_FRA_Pau_Methane_3000ft_Line_10001_162717_000_rdn_csf_results

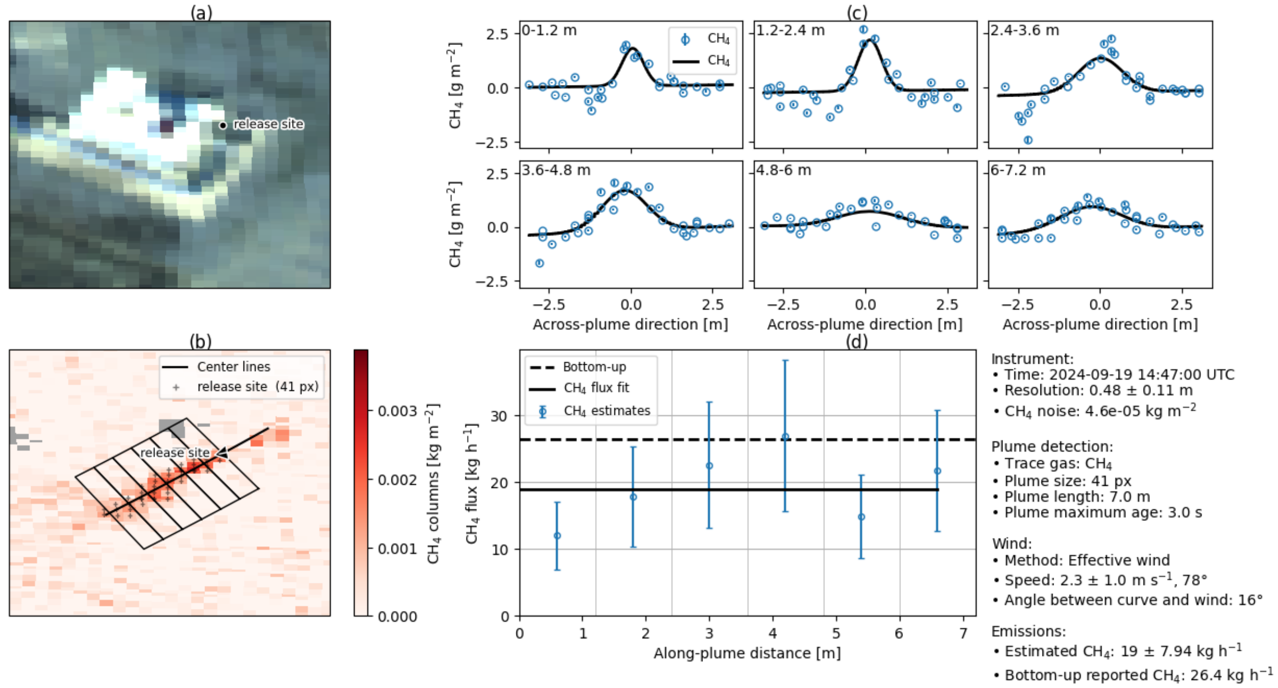

Fig. S61: M017_240919_FRA_Pau_Methane_4200ft_Line_20001_164659_000_rdn_csf_results

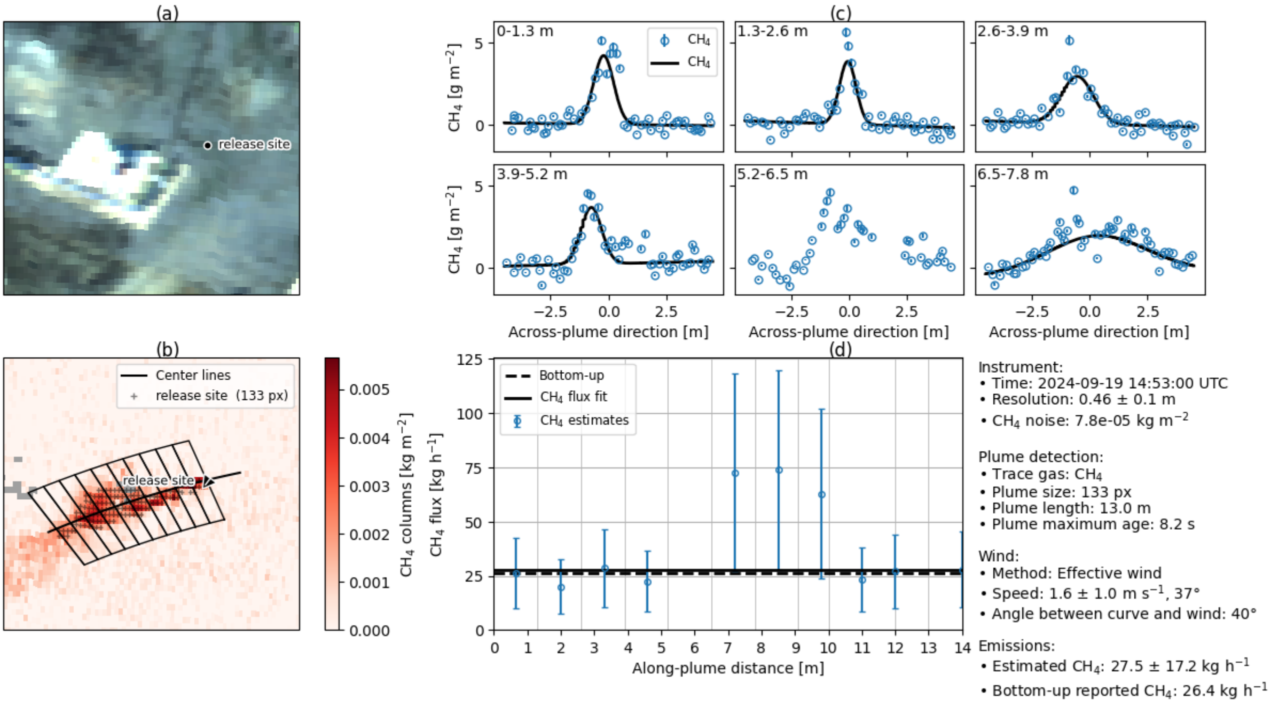

Fig. S62: M017_240919_FRA_Pau_Methane_4200ft_Line_10001_165249_000_rdn_csf_results

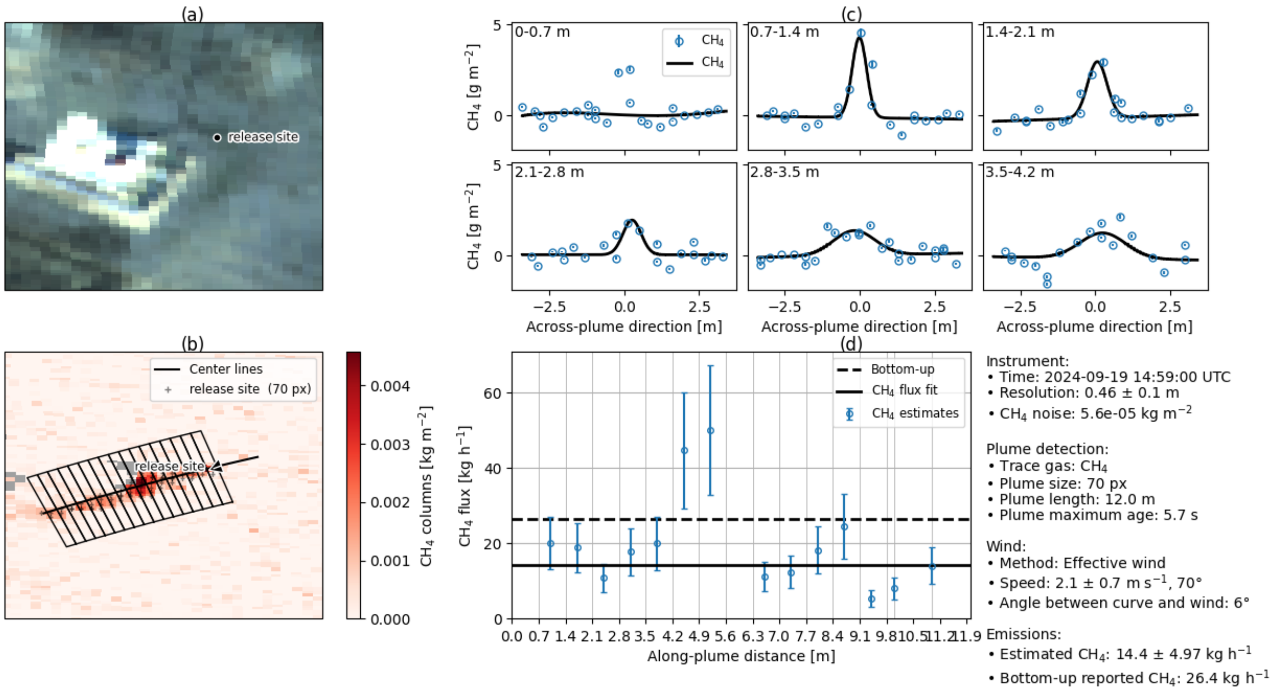

Fig. S63: M017_240919_FRA_Pau_Methane_4200ft_Line_20001_165902_000_rdn_csf_results

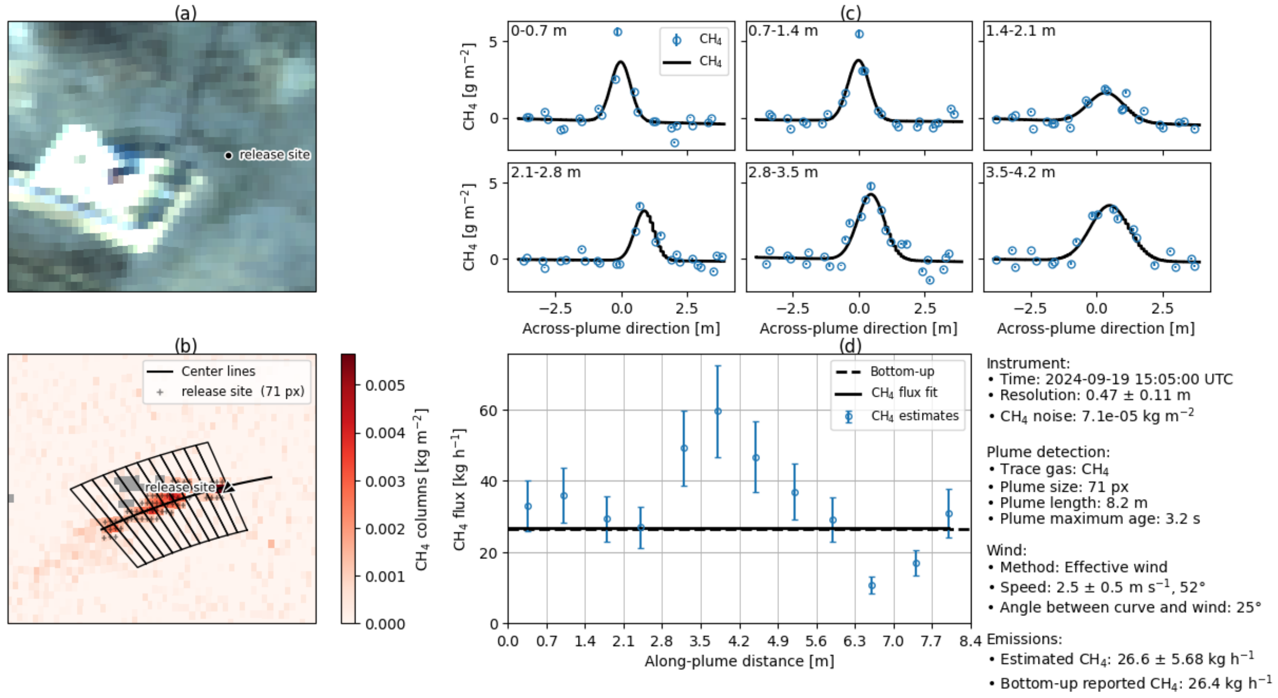

Fig. S64: M017_240919_FRA_Pau_Methane_4200ft_Line_10001_170513_000_rdn_csf_results

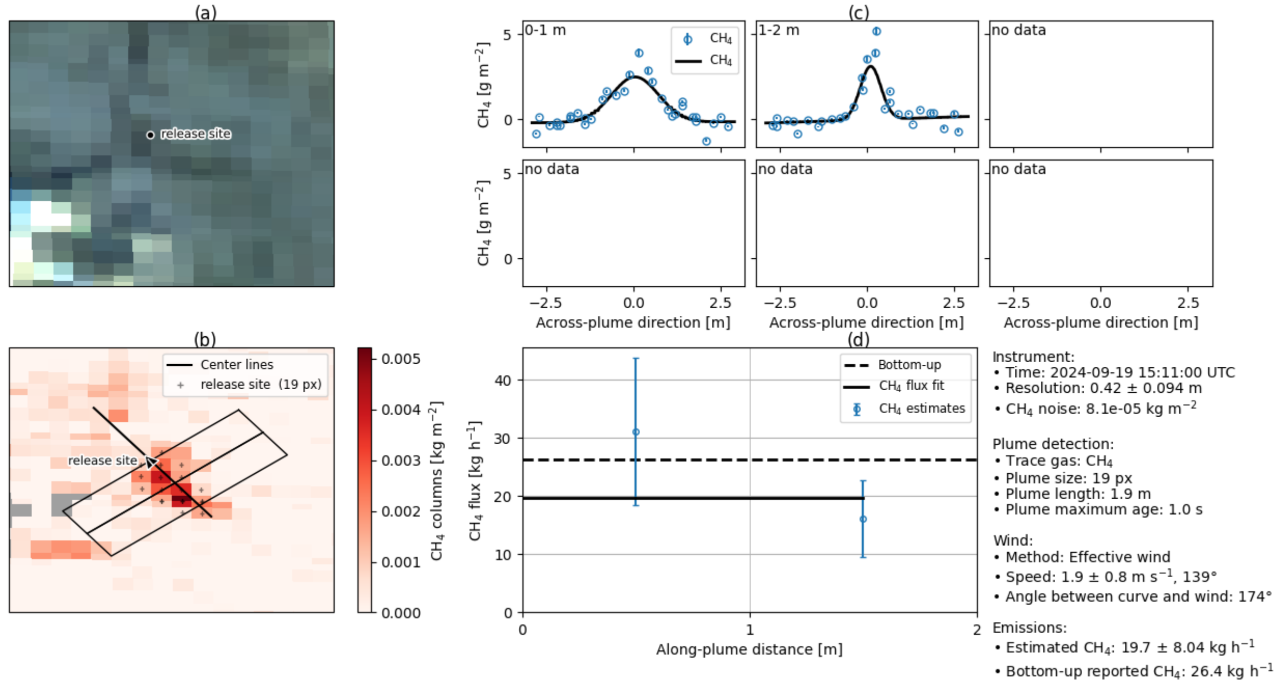

Fig. S65: M017_240919_FRA_Pau_Methane_3000ft_Line_20001_171100_000_rdn_csf_results

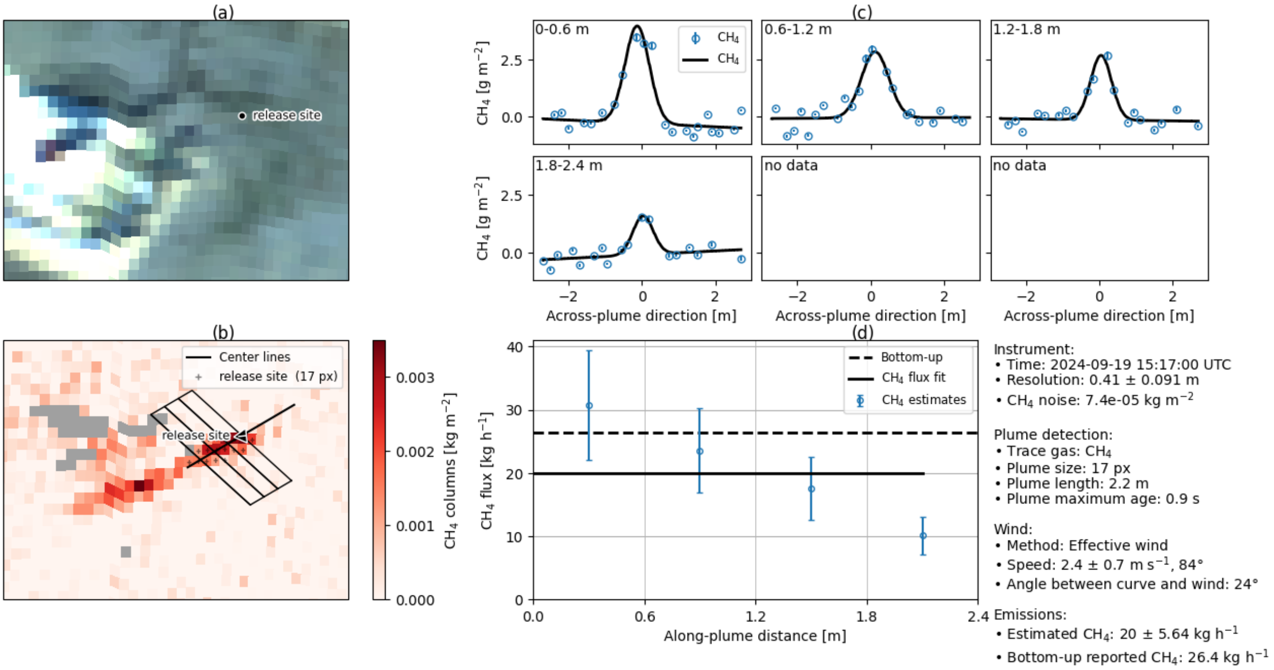

Fig. S66: M017_240919_FRA_Pau_Methane_3000ft_Line_10001_171711_000_rdn_csf_results

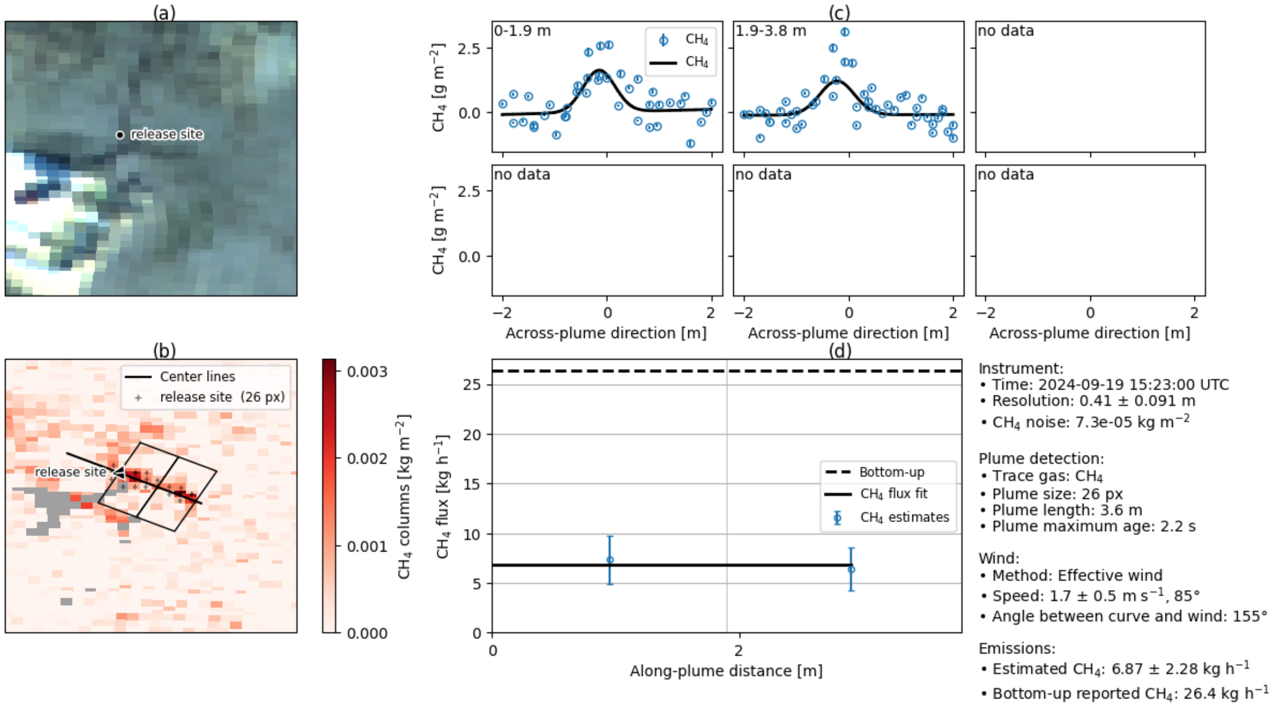

Fig. S67: M017_240919_FRA_Pau_Methane_3000ft_Line_20001_172247_000_rdn_csf_results

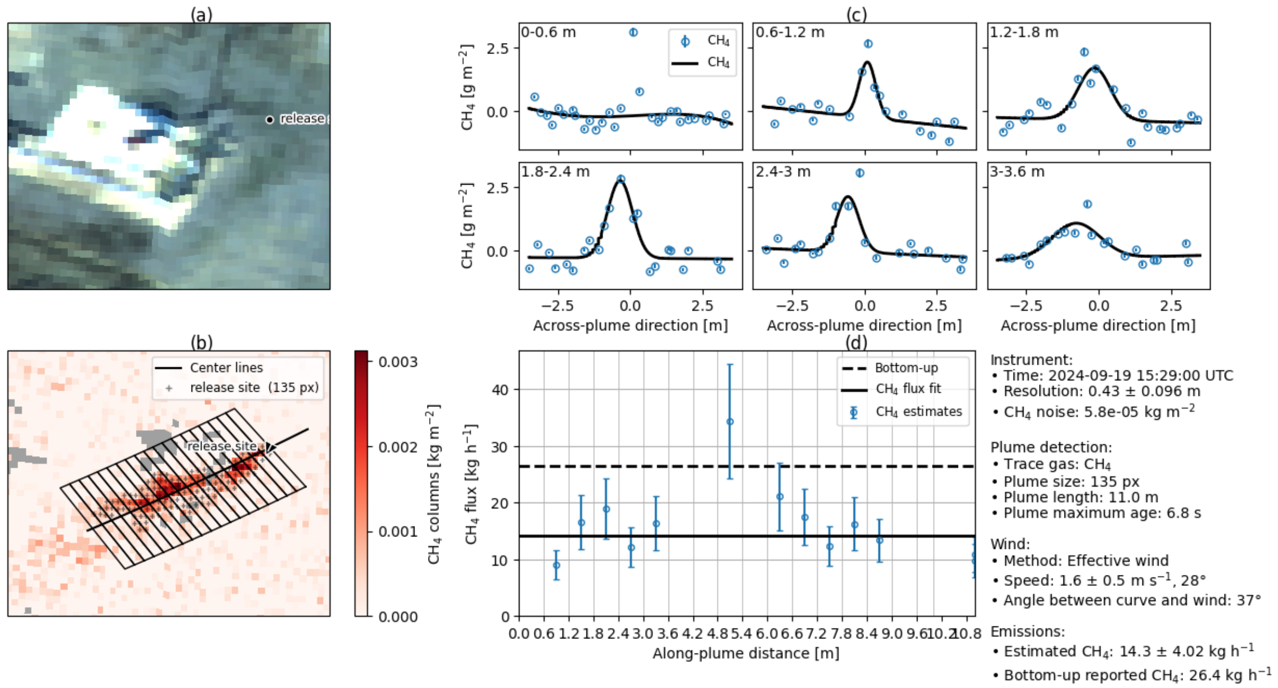

Fig. S68: M017_240919_FRA_Pau_Methane_3000ft_Line_10001_172850_000_rdn_csf_results

Emission estimation metrics for different sources of wind speed

Table S1: RMSE of the emission estimates using different sources of wind speed, according to Figure 8 in the Meier et al., (2025).

Bin	ERA5 U_{10}	Lidar 38m	Lidar 20m	Lidar 10m	U_{10} * 1.47	U_{source}
(0, 15]	1.0694	1.5377	1.5221	1.4081	2.3669	1.0655
(15, 30]	0.371	1.0488	0.6853	0.4106	0.952	0.3134
(30, 100]	0.5871	0.5976	0.5088	0.4223	0.6429	0.5163
(100, 300]	0.5221	0.4193	1.584	1.0375	1.7565	0.5821

Table S2: Table 1: MBE of the emission estimates using different sources of wind speed, according to Figure 8 in the Meier et al., (2025).

Bin	ERA5 U_{10}	Lidar 38m	Lidar 20m	Lidar 10m	U_{10} * 1.47	U_{source}
(0, 15]	0.4848	0.9177	0.9156	0.8445	1.7114	0.3608
(15, 30]	-0.0694	0.647	0.5079	0.2248	0.8005	-0.2246
(30, 100]	-0.2124	0.1666	0.1058	-0.1036	0.3177	-0.4311
(100, 300]	-0.4576	0.0685	0.6451	0.3895	1.0425	-0.1775

Comparison of emission estimates using CSF and IME

We estimated the CH_4 emissions using the IME for the cases where we used the CSF in our manuscript. The opposite was not possible as the CSF cannot be applied to the plumes which do not follow a Gaussian distribution (e.g. overlapping double plumes etc.). This is the reason why we used the IME for these cases in the first place. Consequently, Figure S69 shows the estimate emissions from 53 out of 68 observed plumes.

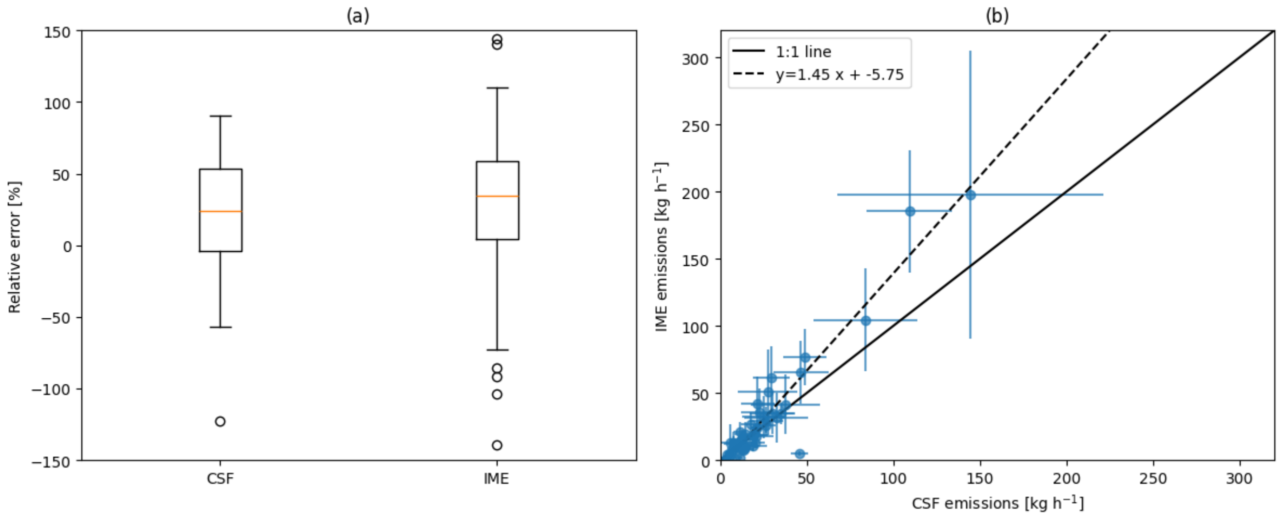

Fig. S69: Comparison of emission estimates using the CSF and IME.

Subplot (a) shows that the relative errors in estimated CH_4 emissions are smaller when using the CSF (median: 24.1%) compared to the IME (median: 34.3%) and that the latter shows a larger spread. As mentioned in the methods section of the paper, this is due to the fact that the CSF is more robust against turbulence than the IME. When comparing the absolute estimated emissions in subplot (b), it becomes evident that the IME tends to result in lower emission estimates than the CSF for small release events. This likely happens because background noise has a larger influence on the integrated CH_4 mass than when using the CSF due to the small integration area. For larger release events, the estimated emissions are higher when using the IME compared to the CSF. This probably occurs because the CSF can better account for local variations of the background by fitting a linear background with the Gaussian curve for each sub polygon.